

On the generation and degradation of emerged coral reef terrace sequences: First cosmogenic ^{36}Cl analysis at Cape Laundi, Sumba Island (Indonesia)

Chauveau Denovan ^{1,*}, Authemayou Christine ¹, Pedoja Kevin ², Molliex Stéphane ¹, Husson Laurent ³, Scholz Denis ⁴, Godard Vincent ⁵, Pastier Anne-Morwenn ⁶, De Gelder Gino ³, Cahyarini Sri Yudawati ⁷, Elliot Mary ⁸, Weber Michael ⁴, Benedetti Lucilla ⁵, Jaud Marion ¹, Boissier Audrey ⁹, Augusta Vera Christanti ⁷, Aribowo Sonny ³, Budd Ann F. ¹⁰, Natawidjaja Danny Hilman ⁷, Aster Team

¹ LGO, IUEM, CNRS, UMR 6538, Université de Bretagne Occidentale, Plouzané, France

² M2C, CNRS, UMR 6143, UnivCaen-Normandie, Caen, France

³ ISTerre, CNRS, UMR 5275, Université de Grenoble Alpes, Grenoble, France

⁴ Institut für Geowissenschaften, Johannes-Gutenberg-Universität Mainz, Mainz, Germany

⁵ CEREGE, CNRS-IRD, UMR 34, Aix-Marseille Université, Aix-en-Provence, France

⁶ GFZ German Research Centre for Geosciences, Earth Surface Process Modelling, Potsdam, Germany

⁷ Research Center for Geotechnology, Indonesian Institute of Science, LIPI, Bandung, Indonesia

⁸ LPG, CNRS, UMR 6112, Université de Nantes, Nantes, France

⁹ IFREMER, Géosciences Marines, Centre de Brest, Plouzané, France

¹⁰ Department of Earth and Environmental Sciences, University of Iowa, Iowa City, USA

* Corresponding author : Deonovan Chauveau, email address : chauveaudenovan@gmail.com

Abstract :

The emerged coral reef terrace sequence at Cape Laundi, on the north coast of Sumba Island (Indonesia), with at least 18 successive strandlines, remains poorly dated in spite of numerous previous data. The age discrepancies within these coral reef terraces (CRTs) were previously explained by their polycyclic nature, triggered by marine erosion and reoccupation of old coral colonies by new ones. This study aims at highlighting these processes, as well as the continental denudation that participates in the partial stripping of the thin superficial coral reef layer overlying the pre-existing surface, exhuming older coral colonies. For this purpose, we use a combined analysis of ^{36}Cl cosmogenic concentrations, new $^{230}\text{Th}/\text{U}$ ages, and previous dating in order to quantify denudation rates affecting the sequence and to highlight the role of marine erosion in reworking the lowest CRT surface. Our results demonstrate that 1) the lowermost CRT is composite, i.e., formed by different reefal limestone units constructed and eroded during successive highstands of the last interglacial, 2) following the last deglaciation, this CRT has been subjected again to coastal erosion and reoccupation during the Mid Holocene highstand, 3) its distal edge is affected by the current marine erosion and shows denudation rates higher by one to two orders of magnitude (from 279 ± 0.4 to 581 ± 0.4 mm ka⁻¹) than the continental denudation values of higher CRTs (14.7 ± 8.3 mm ka⁻¹ on average), 4) at the scale of a single CRT surface, variations in continental denudation rates are caused by epikarstification roughness, and 5) the distal edges have the highest

continental denudation rate due to diffusion and regressive erosion produced by the runoff occurring along the steep downward cliff.

Highlights

► Coral reef terraces at Cape Laundi (Sumba Island) have a polycyclic nature. ► An analysis of ^{36}Cl cosmogenic concentrations on terraces to quantify continental denudation and marine erosion rates. ► Marine erosion and continental denudation explained the age diachronism on a single terrace. ► The lower terraces experienced alternating construction and erosion phases during highstands of the last interglacial. ► Marine erosion rates are much higher by one to two orders of magnitude than the continental denudation rates.

Keywords : Quaternary, Coral reef terrace, Cl-36 cosmogenic isotope, Denudation rate, U-Th series, Coastal erosion, MIS 5, Southeastern asia

54 **1. Introduction**

55

56 Sumba is an actively rising island in Indonesia where an emerged coral reef terraces
57 sequence records the progressive emergence of the island. The sequence at Cape
58 Laundi, on the north coast of the island, reaches ~470 m in elevation and includes at
59 least 18 successive coral reef terraces (CRTs). This sequence has a well-preserved
60 and potentially valuable record of Quaternary sea level, paleoclimate and tectonics, for
61 which dating of the CRTs is crucial. The previous studies of this CRTs sequence
62 (Pirazzoli et al., 1991; 1993; Bard et al., 1996) have identified significant temporal
63 discrepancies within the CRTs, i.e., different ages of corals within the same CRT and
64 similar ages of corals on several CRTs. Pirazzoli et al. (1991; 1993) and Bard et al.
65 (1996) proposed that the CRTs have a polycyclic nature in order to explain age
66 diachronism (Fig. 1). Pirazzoli et al., (1993) suggested that marine erosion can reshape
67 the CRT surface and promote the bioconstruction of a new coral-colony on an older
68 one during sea level highstands (Fig. 1A). Bard et al. (1996) indicated that a decrease
69 in the rate of uplift to a low rate would in recurrent similar relative sea levels, causing
70 several phases of reef development on a pre-existing surface (Fig. 1B). The role of
71 marine erosion on the morphogenesis of CRTs has been discussed since a long time
72 (e.g., Chappell, 1974; Hearty et al., 2008). Despite the persistence in recent
73 publications of a simplistic definition of CRTs as constructive marine terraces; it is now
74 clearly accepted in many syntheses that a CRT surface results from the combination
75 of bioconstruction, erosion at sea level and accumulation of the eroded sediments
76 (Pirazzoli, 2005; Cabioch, 2011; Murray-Wallace and Woodroffe, 2014; Pedoja et al.,
77 2018; Pastier et al., 2019).

78

79 Apart from the role of marine erosion and bioconstruction reoccupation, what is the
80 role of continental denudation in age diachronism on the same CRT? On polycyclic
81 CRT, continental denudation could partially strip the thin superficial layer of a young
82 fossil coral reef and exhume older corals in several places (Fig. 1C). Since the
83 stratigraphy of the CRTs on Sumba is not described and is difficult to observe in the
84 canyons that incise them, and since the preservation of paleo-soils is unlikely in the
85 polycyclic CRTs by their subsequent marine abrasion during a new transgression, we
86 have chosen to combine the cosmogenic ^{36}Cl method (e.g., Lal, 1988; 1991; Bierman,
87 1994), new $^{230}\text{Th}/\text{U}$ dating and previous dating to highlight the processes of marine
88 erosion, reoccupation and continental denudation affecting the CRTs of Cape Laundi.
89 The ^{36}Cl method has already been carried out on CRTs in Barbados, resulting in
90 quantification of the continental denudation rate (Lal et al., 2005).

91

92 In this study, we measured the cosmogenic ^{36}Cl isotopes concentration of 34 *in situ*
93 surface samples collected from the oldest CRT to the current reef shelf and took
94 several samples on each CRT from the inner edge to the lower cliff in order to detect
95 variation of continental denudation on them (Figs. 1C; 2). Moreover, we analyzed the
96 ^{36}Cl concentration in a 2.5 ± 0.1 m deep core of the lowermost CRT to attempt to (1)
97 constrain its exposure time to cosmic rays (i.e., the age at which it emerged) if the
98 concentration of ^{36}Cl decreases exponentially at depth (e.g., Braucher et al., 2011), or
99 (2) to detect several exposure phases (i.e., reoccupation stages) by ^{36}Cl concentration
100 peaks at depth (Figs. 1A; 1B). We conducted $^{230}\text{Th}/\text{U}$ dating of two coral colonies in
101 growth position collected on the Holocene landform and used these $^{230}\text{Th}/\text{U}$ ages to
102 calculate a coastal denudation rate from the ^{36}Cl concentrations of samples taken from
103 the top of the active Holocene sea cliff. We discuss our results in terms of 1) their

104 comparison with global trends, as well as 2) continental denudation rates of carbonates
105 and their heterogeneity, and 3) the influence of marine erosion and constructive
106 reoccupation components on CRT morphogenesis.

107

108 **2. Background**

109 **2.1. Emerged coral reef terrace sequences**

110

111 Morphologically, a CRT is an expanse of reefal limestone with a surface that is flat or
112 slightly sloping seawards, limited by a change in slope seaward and landward.
113 Seaward, the change in slope (i.e., a distal edge associated with a more or less steep
114 cliff; Fig. 2), is usually described as the paleo reef crest (e.g., Pirazzoli et al., 1991;
115 Rovere et al., 2016). Landward, at the inner edge, a CRT is characterized by a break
116 in slope, sometimes interpreted as a shoreline angle suggesting the erosional sea cliff
117 nature (e.g., Speed and Cheng, 2004; Pedoja et al., 2018). This break in slope provides
118 a rather good marker for relative sea level, usually associated with the sea level
119 highstands of former interglacial stages (e.g., Pirazzoli et al., 1993; Bard et al., 1996;
120 Pedoja et al., 2018).

121

122 CRTs are geomorphologic plane surfaces encountered in the tropical zones and are a
123 type of marine terraces in the broadest sense of the term (Schwartz, 2006; Murray-
124 Wallace and Woodroffe, 2014; Pedoja et al., 2018). When the global sea level falls too
125 rapidly and/or the reef is lifted by tectonic movements or glacial isostatic adjustment, it
126 emerges, dies, and fossilizes, forming a CRT. The joint effects of sea level oscillations
127 and tectonic uplift can result in the generation of a CRTs sequence with a staircase
128 geometry (Fig. 2) (e.g., Chappell, 1974; Pirazzoli, 2005). Since the 19th century, such

129 sequences have been described in the Caribbean province (Haiti, Cuba, Barbados;
130 e.g., Crosby, 1883; Simms, 2021; Thompson and Creveling, 2021), in the Indo-Pacific
131 province (Indonesia, Papua New Guinea, Japan, Fiji, Philippine, and other islands or
132 archipelagos; e.g., Darwin, 1842; Daly, 1915; Pirazzoli et al, 1993; Pedoja et al, 2018),
133 as well as alongshore the Red Sea (Scholz et al., 2004; Murray-Wallace and
134 Woodroffe, 2014; Pedoja et al., 2011; 2014; Obert et al., 2019).

135

136 The stratigraphy and morphology of a CRT, as well as these of a sequence, result from
137 interactions between the vertical land motion, absolute and relative sea level
138 variations, slope of the foundations, erosion processes (either mechanical or chemical
139 and marine or continental in origin), reef bioconstruction, subsequent accumulation of
140 eroded sediments and reef reoccupation (e.g., Pirazzoli, 2005; Cabioch, 2011; Husson
141 et al., 2018; Pedoja et al., 2018; Pastier et al., 2019). Rates of reef growth, marine
142 erosion and sedimentation may vary spatially due to a change in shoreline direction
143 (e.g., from a bay to a cape), resulting in a modification in the final geometry of the
144 sequence (Fig. 2). Thus, one CRT with a continuous high fossil sea cliff (>10 m; CRT
145 I in figure 2) can include numerous secondary or intermediate CRTs (CRTs I₁ and I₂ in
146 figure 2) with or without low (<10 m), eroded, fossil sea cliffs and various reefal
147 limestone units (Fig. 2) (Hantoro et al., 1989; Pirazzoli et al., 1993; Speed and Cheng,
148 2004). Geomorphologically, these compound CRTs are named main CRTs (e.g.,
149 Pirazzoli et al., 1993). These main CRTs, sometimes morphologically forming a single
150 CRT (CRT I in figure 2), may contain coral colonies sampled in growth position on their
151 surface providing ages associated with different Marine Isotope Stage (MIS) (the
152 different reefal limestone units on CRT I in figure 2) (e.g., Pirazzoli et al., 1993; Bard

153 et al., 1996). When such a diachronism is observed, these CRTs are named composite
154 CRTs (e.g., Kindler et al., 2007).

155

156 **2.2. Sumba Island**

157 **2.2.1. Tectonic and geologic setting**

158

159 Sumba is a 220 km-long and 65 km-wide island located in the lesser Sunda
160 Archipelago, Indonesia. It is located near the transition from oceanic subduction in the
161 West, along the Java trench, to the collision of the Banda arc with the continental
162 Indian-Australian plate in the East (Fig. 3) (Hinschberger et al., 2005). The Cretaceous
163 to Oligocene crystalline basement is almost entirely covered by Miocene and Pliocene
164 deposits (Abdullah et al., 2000). The Miocene rocks consist of carbonate platform
165 deposits to the west that evolve eastward into deep basin deposits (Von der Borch et
166 al., 1983; Van der Werff et al., 1995). Since the late Miocene/Pliocene, the
167 convergence between the Eurasian and Indian-Australian plates has been driving
168 shortening and uplift in the fore-arc domain (e.g., Harris, 1991; Fortuin et al., 1997;
169 Haig, 2012; Tate et al., 2014). In Sumba island, the Quaternary uplift is recorded by a
170 ~350 km long CRTs sequence (e.g., Pirazzoli et al., 1991; Bard et al., 1996). The
171 Sumba sequence is nearly continuous, interrupted only locally by large rivers. It spans
172 approximately two-thirds of the island's shores, mostly along its northern coast and the
173 eastern and western tips of the island (Hantoro, 1992; Fleury et al., 2009; Nexer et al.,
174 2015; Authemayou et al., 2018).

175

176 **2.2.2. Climate and hydrodynamics**

177

178 The climate affecting Sumba island is tropical, with humid winters and dry summers,
179 albeit relatively dry compared to other parts of Indonesia (Prasetia et al., 2013). The
180 mean annual precipitation in Sumba is 1077 ± 406 mm a⁻¹ (average over the 1998-
181 2009 period of TRMM data; e.g., Kummerow et al., 2000).

182

183 The tides of Sumba Island have a range of ~3.5 m (Colas and Sutherland, 2001;
184 Alfonso-Sosa, 2016; Hibbert et al., 2016). Nevertheless, our study site (Cape Laundi)
185 is located on the northern, leeward side of the island which is only exposed to short
186 wavelength fetch swell (<10 s, i.e., windswell) (Butt et al., 2004).

187

188 **2.2.3. Previous studies on the Cape Laundi emerged coral reef**

189 **terraces sequence**

190

191 Cape Laundi was first mapped by Jouannic et al., (1988). It reaches ~470 m in
192 elevation and has a staircase shape with six main CRTs separated by continuous high
193 (>10 m) fossil sea cliffs (Pirazzoli et al., 1993). Each main CRT includes several
194 intermediate CRTs (Hantoro et al., 1989; Pirazzoli et al., 1993). Marine erosion was
195 detected by Pirazzoli et al. (1991; 1993) from the presence of marine notches in the
196 inner edges of main CRTs, and the observation of coral development surfaces marked
197 by traces of subsequent erosion observed along several canyons transversely cutting
198 the slope of the sequence.

199

200 Approximately fifty coral colonies have been dated (using U/Th and ESR dating
201 methods) on the surface of the five lowest main CRTs (T_I to T_{IV1} in Pirazzoli et al.,
202 1993). These ages were correlated to eustatic peaks of the highstands associated,

203 respectively from the oldest to the youngest, to MIS 15 (610 ± 10 ka), MIS 11 ($390 \pm$
204 30 ka), MIS 9 (325 ± 18.5 ka), MIS 7 (239.5 ± 8.5 ka), MIS 5 (122 ± 6 ka) and MIS 1
205 (mid Holocene highstand, 6 ± 2 ka) (Pirazzoli et al., 1993; Bard et al., 1996). The oldest
206 dated CRT, named T_{IV1} in previous studies, yielded ESR ages of 584 ± 88 ka and 603
207 ± 90 ka and was corresponding to MIS 15 (Pirazzoli et al., 1991; 1993). At higher
208 elevations than T_{IV1} , the ages of the successive CRTs were extrapolated assuming a
209 constant uplift rate (i.e., 0.49 ± 0.01 mm a^{-1} ; Pirazzoli et al., 1993). The upper, undated
210 CRTs were thus correlated to sea level highstands up to ~ 1 Ma, i.e., MIS 29 (Jouannic
211 et al., 1988; Pirazzoli et al., 1991; 1993; Hantoro, 1992; Bard et al., 1996).

212

213 However, a number of temporal discrepancies emerged with the dating done by
214 Pirazzoli et al. (1991; 1993). Firstly, U-series ages of corals from the same CRT are
215 diachronic (e.g., ages of ~ 82 ka and ~ 138 ka from CRT I_1). Secondly, the same U-
216 series ages came from corals on at least three CRTs (e.g., MIS 5e ages on CRTs I_1 ,
217 I_2 , and II_2), and thirdly, U-series ages and ESR ages of corals from the same CRT do
218 not always match with one another. Thereafter, TIMS U-series dating of corals (Bard
219 et al., 1996) specified the diachronism (i.e., MIS 5a, 5c, and 5e ages on CRT I_1 ; MIS
220 5c, 5e and pre-MIS 5e ages on CRT I_2).

221

222 Bard et al. (1996) interpreted the age inconsistencies to reflect the decrease in uplift
223 rates during a significant period of the late Pleistocene. Very low uplift rates induce
224 negligible uplift of the lowest CRTs before the next transgression, resulting in one or
225 more reoccupation events in which new coral can grow on the pre-existing CRT (Fig.
226 1B). Combining $^{230}\text{Th}/\text{U}$ dating with numerical modeling, Bard et al. (1996) estimated
227 an uplift rate ranging from 0.2 to 0.5 mm a^{-1} and proposed also a polycyclic nature for

228 several CRTs (up to MIS 7). Low uplift rates (0.2 mm a^{-1}) allow coral colonies of a CRT
229 to be recovered by younger ones during a new transgression. But, to obtain the 0.2
230 mm a^{-1} minimum uplift rate, the previous authors correlated the inner edge of the
231 lowermost main CRT ($23 \pm 2 \text{ m}$) to MIS 5e, taking into account only the oldest $^{230}\text{Th/U}$
232 ages. This hypothesis implies that during the MIS 5c and 5a highstands, coastal
233 erosion has been negligible to preserve the morphology of the MIS 5e CRT.

234

235 Pirazzoli et al. (1993) interpreted the age inconsistencies to reflect marine erosion.
236 Indeed, they suggested that eustatic sea level fluctuations with efficient marine
237 abrasion superimposed on a regular uplift trend of 0.5 mm a^{-1} must have led sea level
238 to reach nearly the same position several times and the development of
239 bioconstructions differing in age as much as 100 ka on the same CRT (Fig. 1A). The
240 present altitude of dated CRTs allowed Pirazzoli et al. (1991; 1993) to propose an uplift
241 rate trend of $0.49 \pm 0.01 \text{ mm a}^{-1}$.

242

243 **3. Methods**

244 **3.1. Mapping, bathymetry, and sampling**

245 **3.1.1. Onshore and offshore data**

246

247 We mapped the inner edges of the CRTs at Cape Laundi using a high resolution (2 m)
248 Digital Elevation Model (DEM) produced from stereoscopic satellite images (Pleides,
249 CNES) with MicMac freeware (e.g., Rupnik et al., 2016). We acquired topographic and
250 bathymetric profiles, using a real kinematic differential global positioning system (RTK
251 DGPS) onshore, and a Humminbird 700 series sonar offshore (Fig. 4). Onshore, our
252 profiles were carried out perpendicular to the main inner edges of the successive

253 CRTs, parallel to those proposed by Pirazzoli et al. (1993) and starting from the mean
254 sea level. Profile 1 crosses the whole CRTs sequence and Profile 2 focuses on the
255 lowest CRTs (Fig. 4).

256

257 The roughness of the successive CRTs increases with elevation and therefore age
258 because of continental denudation (e.g., epikarst). This roughness is the main source
259 of error in elevation, far beyond instrumental errors. Consequently, we assigned an
260 elevation uncertainty to all the field measurements as a function of the amplitude of the
261 observed natural landform roughness; ± 0.5 m for low standing landforms ($<250.5 \pm$
262 0.5 m in elevation); ± 1.5 m on the summit of Cape Laundi and the upper CRTs (>250.5
263 ± 0.5 m in elevation) (Fig. 5).

264

265 **3.1.2. Sampling strategy**

266

267 We extracted samples for $^{230}\text{Th}/\text{U}$ dating, by drilling two coral colonies in growth
268 positions (samples SUM17-10 and SUM17-13) located on the Holocene CRT (H), near
269 the modern shore (Figs. 3; 4). From the base (CRT H) to the summit of Cape Laundi
270 (CRT VI), we collected 34 samples from the non-vegetated surfaces of the reefal
271 limestones forming the CRTs for cosmogenic ^{36}Cl analysis (Figs. 3; 4). To investigate
272 the potential variability of denudation rates across a given CRT, we collected samples,
273 when possible, from 1) the inner edge, 2) the main surface and 3) the distal edge (Fig.
274 2).

275

276 Below 167.6 ± 0.5 m, intermediate CRTs are distinguishable in the field through fossil
277 sea cliffs (~ 3 m in height), separated by narrow (80-430 m wide) flat surfaces (Fig. 6).

278 For such CRTs, the distances between two successive sampling sites (i.e., inner edge,
279 main surface, and distal edge) typically range from 20 to 100 m. The CRTs higher than
280 167.6 ± 0.5 m are wider, typically from ~330 to ~1 300 m wide, and our sampling
281 interval is ~500 m.

282

283 To constrain exposure age (i.e., the age at which the CRT emerged), in the case that
284 the concentration of ^{36}Cl decreases exponentially at depth (e.g., Braucher et al., 2011)
285 or to highlight several exposure events (i.e., reoccupation stages), in the case that ^{36}Cl
286 concentration peaks at a certain depth, we drilled the lowermost CRT (I₁) to get a
287 continuous ~2.5 m deep borehole (Fig. 4) (e.g., Braucher et al. 2009; 2011; Hein et al.
288 2009; Schaller et al. 2009). Because of the heterogeneity and porosity of the fossil
289 reefal limestone, our borehole broke into pieces, preventing us from precisely knowing
290 the depths of most of the individual samples. Only the depth of the deepest material
291 recovered from 2.5 ± 0.1 m below the surface of the CRT and the surface sample were
292 considered.

293

294 **3.2. Cosmogenic nuclides**

295

296 The ^{36}Cl cosmogenic concentration in rocks ($N(z,t)$, g^{-1} atom) as a function of depth (z ,
297 cm) and time (t , year) can be expressed as follows (Stone et al., 1994):

298

$$299 \frac{\partial N(z,t)}{\partial t} = P(z) - \lambda N(z,t) - \varepsilon \frac{\partial N(z,t)}{\partial z} \quad (1)$$

300

301 z is the depth of a sample. Here, all but one sample (from the bottom of the core in the
302 lowermost CRT) have been collected from exposed bedrock surfaces ($z=0$), under a

303 surface that denudes at a rate ϵ (cm a^{-1}). $P(z)$ is the total production rate of ^{36}Cl (atom
304 $\text{g}^{-1} \text{rock a}^{-1}$), depending on 1) the cosmic radiation (itself affected by the following
305 parameters: latitude, elevation, topographic shielding, self-shielding (i.e., sample
306 thickness and depth)) passing through a rock of thickness z and 2) on the composition
307 of the rock (Gosse and Phillips, 2001). λ is the decay constant of ^{36}Cl ($\lambda = 2.303 \cdot 10^{-6}$
308 a^{-1}).

309

310 For all 34 samples, we selected the carbonate matrix containing as few coral fragments
311 as possible. Density measurements on these matrix samples averaged 2.5 g cm^{-3} .
312 Each sample was washed and the fraction 250-1000 μm extracted. About $\sim 100 \text{ g}$ of
313 each sample was then used for chemical analysis. We used a standard chlorine
314 extraction protocol, which includes several steps of leaching, designed to remove labile
315 Cl of meteoric origin from mineral surfaces (Stone et al., 1996; Merchel et al., 2008;
316 Schlagenhauf et al., 2010). More precisely, the procedure involved a cleaning process
317 by ultrapure water to remove any suspended particles, followed by a partial dissolution
318 process in 2M HNO_3 . Samples were then spiked with $\sim 270 \mu\text{g}$ of an enriched $^{35}\text{Cl}/^{37}\text{Cl}$
319 solution in order to determine the ^{35}Cl natural content. Then, the sample was fully
320 dissolved in 2M HNO_3 . Residues were filtered from the solution and weighted. 1 ml
321 solution aliquot was collected from the filtered solution for Ca determination. Then, Cl
322 was precipitated as AgCl using AgNO_3 . The precipitate was dissolved with ammonia
323 and sulfur was reduced by the addition of a saturated $\text{Ba}(\text{NO}_3)_2$ solution. Afterwards,
324 the solution was filtered and a second precipitation of AgCl was performed with HNO_3 .
325 The dried AgCl was finally measured with Accelerator Mass Spectrometry (AMS) at
326 CEREGE (Centre de Recherche et d'Enseignement de Géosciences de
327 l'Environnement) in Aix-en-Provence (France). ^{36}Cl production and denudation rates

328 were calculated following Schimmelpfennig et al. (2009) taking into account Sea-Level-
329 High-Latitude production rates for rapid neutron spallation reactions (42.2 ± 2 atoms
330 ^{36}Cl (g $\text{Ca}^{-1} \text{a}^{-1}$); Braucher et al., 2011; Schimmelpfennig et al., 2011; 2014), negative
331 muons (Heisinger et al., 2002), the rate of epithermal neutron production from fast
332 neutrons (Phillips et al., 2001) and the production from radiogenic neutrons (Fabryka-
333 Martin, 1988; Phillips and Plummer, 1996) (more information related to ^{36}Cl production
334 is detailed in Appendix "A" of Schimmelpfennig et al., 2009). Topographic shielding
335 was calculated for each sample using the topographic shielding add-in for ArcGIS
336 software (Codilean, 2006). The scaling factors are calculated with CosmoCalc 1.7
337 macro (Vermeesch, 2007; Dunai, 2010). Major oxides (SiO_2 , TiO_2 , Al_2O_3 , Fe_2O_3 , MnO ,
338 MgO , CaO , Na_2O , K_2O , P_2O_5) and trace elements (Li, Be, Mo, Ba, Sm, Gd, Pb, Th, U,
339 B, Sc, Cr, Cr, Co, Ni, Rb, Sr) have been measured on the bulk samples (i.e., the size
340 fraction $< 250 \mu\text{m}$ collected after crushing), respectively by an ICP AES-Ultima 2-Jobin
341 Yvon and an HR-ICP-MS Element XR, at the LGO (Laboratoire Géosciences Océan,
342 IUEM) in Brest (France) to determine their impact on the ^{36}Cl production rate. The CO_2
343 concentration in samples is determined by weighing the samples, dissolving them in a
344 Gas bench and measuring the CO_2 produced (Pôle de Spectrométrie Océan,
345 Plateforme Isotopes Stables, IUEM, Brest, France).

346

347 The interaction of secondary cosmic rays with rocks exposed in the Earth's surface
348 produces cosmogenic isotopes (Gosse and Phillips, 2001). Four major interactions are
349 responsible for the production of cosmogenic isotopes, in order of importance:
350 spallation, muon capture, neutron activation, and alpha particle interaction (Bierman,
351 1994). Except for the production of ^{36}Cl by neutron capture, which peaks at a shallow
352 depth rather than at the surface, cosmogenic isotope production rates decrease

353 exponentially with depth until they stabilize (Stone et al., 1998). The abundance of
354 cosmogenic isotopes increases with exposure time until steady state, when production
355 and decay of the cosmogenic isotope are balanced (Schlagenhauf et al., 2010). More
356 precisely, when bedrock surfaces are exposed to cosmic ray particles and denuded at
357 a constant rate for long enough, the induced cosmogenic nuclide production
358 equilibrates the losses due to radioactive decay and mass removal linked to
359 denudation processes (Lal, 1991). The cosmogenic nuclide concentration reached at
360 this steady state is inversely proportional to the denudation rate of the surface (e.g.,
361 Granger and Riebe, 2014). The time it takes for the concentration of a cosmogenic
362 nuclide to reach steady state depends mainly on the denudation rate. When this steady
363 state is reached, it is possible to quantify the denudation rates without knowing the age
364 of the surface because for any age taken, and for a given ^{36}Cl concentration, the
365 denudation rate will not vary anymore (e.g., Lal et al., 1991; Dunai, 2010). Conversely,
366 for a surface sample that has not reached steady state and was taken on a surface
367 without age constraint, there is an infinite number of age-denudation pair hypotheses
368 that can explain the measured concentration. The denudation rate can be calculated
369 by assuming or independently constraining an exposure age (e.g., using absolute
370 chronological constraints such as $^{230}\text{Th}/\text{U}$ ages) and vice versa. Also, constraining both
371 exposure ages and denudation rates when steady state is not reached is possible by
372 fitting a theoretical depth profile, calculated from measured surface and depth
373 concentrations (Braucher et al. 2009; 2011; Hein et al. 2009; Schaller et al. 2009).

374

375 In this study, the denudation rates were calculated from ^{36}Cl concentrations assuming
376 a range of absolute ages for CRTs proposed by Pirazzoli et al. (1991; 1993). We show
377 that cosmogenic steady state has been reached for older CRTs than CRT Il₇

378 (corresponding to ~137 m altitude; Fig. 6) because denudation rates remain
379 unchanged regardless of the chosen age for the CRT. Thus, the age hypotheses are
380 useless to quantify denudation rates for these older CRTs (Section 4.4.). Samples on
381 CRTs surfaces yield continental denudation rates (Fig. 1C), while samples from CRT
382 H yield the quantification of marine erosion (Fig. 1A). Denudation rates are averaged
383 over the time period necessary to erode to a depth equivalent to the neutron
384 characteristic attenuation length (approximately 60 cm in a substrate with a density of
385 2.5 g cm^{-3}) (Von Blanckenburg, 2005).

386

387 **3.3. $^{230}\text{Th}/\text{U}$ dating**

388

389 On CRT H (Holocene), at the same sites as the lowest ^{36}Cl samples (SUM18-46 and
390 SUM18-47), we also sampled coral colonies of *Platygyra* (sample SUM17-10) and
391 *Favites* (sample SUM17-13 drilled in a fossil tidal pool) in growth position for $^{230}\text{Th}/\text{U}$
392 dating (Fig. 4). These $^{230}\text{Th}/\text{U}$ dating were done on CRT H in order to complete the
393 bibliographic data and to be as close as possible to the cosmogenic nuclide samples
394 to better discuss marine erosion processes. The two samples were mechanically
395 cleaned with a micro-drill and then crushed. Coral samples were rinsed in MilliQ water
396 and leached in 0.1 N bi-distilled HCL for 15-20 minutes in an ultrasonic bath. The
397 cleaned samples were then crushed into powder and analyzed using a XRD Bruker
398 D8 at the LCG (Laboratoire d'étude des "Cycles Géochimiques et Ressources",
399 IFREMER) in Brest (France) to quantify the relative quantities of calcite and aragonite.
400 We proceeded with $^{230}\text{Th}/\text{U}$ dating only with two samples, consisting purely of
401 aragonite (>99%).

402

403 Subsequently, the powders were dissolved in 7N HNO₃ and a mixed ²²⁹Th-²³³U-²³⁶U
404 spike was added to the solution and allowed to equilibrate. A detailed description of
405 the calibration of the spike is given by Gibert et al. (2016). After drying down the
406 solutions, the residues were treated with a mixture of concentrated HNO₃, HCl, and
407 H₂O₂ to remove potential organic components. Then, the solutions were dried again
408 and dissolved in 6N HCl. The fractions of U and Th were then separated from the
409 CaCO₃ matrix as described by Yang et al. (2015). For mass spectrometric analysis,
410 the U and Th fractions were dissolved in 2 ml of 0.8N HNO₃. U and Th isotope analysis
411 was performed by multi-collector inductively coupled plasma mass spectrometry at the
412 Institute for Geosciences of the Johannes Gutenberg-University, Mainz (Germany),
413 using a Thermo Fisher Scientific Neptune Plus MC-ICP-MS. A detailed description of
414 the analytical procedures is given by Obert et al. (2016).

415

416 **4. Results**

417 **4.1. Cape Laundi: offshore and onshore landforms**

418

419 Improved DEM resolution, new bathymetric data and field observations allowed us to
420 improve the mapping of Cape Laundi. The precise description of the coastal
421 morphology is essential to better understand the processes of its formation and
422 destruction. Offshore, two submerged ~200 m wide surfaces (named -I₁ and -I₂; Fig. 6),
423 were newly identified. Their morphology is consistent with paleo-lagoons: flat in their
424 central part (at -38 ± 1 and -53 ± 1 m for -I₁ and -I₂, respectively; Fig. 6) and convex at
425 their distal part associated with submerged barrier reefs (at -31 ± 1 and -44 ± 1 m for -
426 I₁ and -I₂, respectively; Fig. 6). We interpret these bathymetric features as submerged
427 CRTs.

428

429 Onshore, seven main CRTs were identified up to 469.8 ± 1.5 m with six major fossil
430 sea cliffs (Figs. 4; 5A; 6). Most of these main CRTs include intermediate CRTs. For
431 example, CRT II, with an inner edge raised at 136.8 ± 0.5 m, is composed of seven
432 intermediate CRTs (II₁, II₂, II₃, II₄, II₅, II₆, II₇) separated by low fossil sea cliffs (<10 m
433 each). The lowermost main CRT (CRT I) is 550 m wide, has an inner edge raised at
434 23.2 ± 0.5 m, and includes of two intermediate CRTs (I₁, I₂) separated at 6.4 ± 0.5 m
435 by a ~3 m high fossil sea cliff. On profile 2, CRT I is only 200 m wide, its surface is
436 irregular, and the two intermediate CRTs (I₁, I₂) are separated at 7.6 ± 0.5 m by a ~15
437 m high fossil sea cliff.

438

439 CRT I₁ consists of well-preserved smooth flat surfaces (Figs. 5C; 5D). In places, its
440 surface is covered by centimeter-scale remnants of a sandstone layer including coral
441 rubbles (Fig. 5E). The surface of CRT I₂ is irregular and exhibits some isolated smooth
442 multi-centimetric carbonate surfaces attesting for the relatively quick formation of rough
443 surfaces on the CRT. This superficial layer becomes rougher and thicker from CRT II₂,
444 where it reaches ~20 cm (Fig. 5B). At the highest CRTs, epikarstic roughness reaches
445 1 to 2 m (Figs. 5F; 5G). Moreover, the roughness varies across the CRTs, between
446 ~0.1 to ~2 m, i.e., the inner edges and the main surfaces of the CRTs are rather smooth
447 whereas their distal edges are rougher (Fig. 5G).

448

449 Alongshore, Holocene landforms are represented by a conglomerate, remnants of
450 limestone banks of fossil reef, and coral colonies in growth position, reaching
451 approximately 2 ± 0.5 m above mean sea level (Fig. 5C). Remnants of CRT H have a
452 restricted width (~5 m) and are delimited seaward by active sea cliffs (Fig. 5C). On the

453 flat surface of CRT H, some fossil corals appear very well-preserved and most
454 frequently located in circular depressions with their associated ramparts filled by a
455 white and fresh carbonated matrix (Fig. 5I). The diameter of such circular landforms is
456 generally ~1 m and we interpret them as fossil tidal pools (Fig. 5I) (Hoeksema, 2012).
457 Fossil coral colonies samples within this Holocene emergent reef have been previously
458 cross-dated from 2.03 ± 0.18 to 6.32 ± 0.14 (Jouannic et al., 1988; Pirazzoli et al.,
459 1991, 1993; Bard et al., 1996). The modern reef flat (called I₀ on Fig. 5B) is typical of
460 a fringing reef, as previously interpreted by Bard et al. (1996). There are living corals
461 on the reef crest (seaward), whereas landwards the reefal flat is covered by coral
462 rubbles (Fig. 5J) and associated with beaches and/or mangroves at some sites.

463

464 **4.2. ²³⁰Th/U dating of the Holocene CRT**

465

466 The two fossil coral samples display ²³⁸U concentrations between 2.4 and 3 ppm (Table
467 1). Low ²³²Th contents together with high (²³⁰Th/²³²Th) activity ratios argue for a lack of
468 significant detrital contamination. Both samples display initial $\delta^{234}\text{U}$ values that agree
469 within errors with a mean modern ocean water value of $\delta^{234}\text{U} = 146.8 \pm 0.1\text{‰}$
470 (Andersen et al., 2010), indicating closed system evolution and no evidence for
471 diagenetic alteration. These coral colonies samples yielded ²³⁰Th/U ages of 5.45 ± 0.02
472 ka (sample SUM17-10) and 2.13 ± 0.01 ka (sample SUM17-13) (Table 1).

473

474 **4.3. Distribution of ³⁶Cl concentration at the scale of the emerged coral** 475 **reef terraces sequence**

476

477 The ^{36}Cl concentrations obtained from the samples along profiles 1 and 2 range from
478 3.68 ± 0.08 to $20.00 \pm 0.37 \cdot 10^5$ atoms g^{-1} rock and average at $7.74 \pm 3.67 \cdot 10^5$ atoms
479 g^{-1} rock ($n = 28$; Table 2). Given the overall uniform lithology and precipitation rate, the
480 variability across the profile is higher than expected if all measured ^{36}Cl concentrations
481 have been controlled by steady erosion. The six measured ^{36}Cl concentrations of
482 samples from CRT I have low variability (with an average at $5.54 \pm 0.67 \cdot 10^5$ atoms g^{-1}
483 rock) compared to the ^{36}Cl concentration of all other/older samples (with an average
484 at $8.25 \pm 3.90 \cdot 10^5$ atoms g^{-1} rock). The ^{36}Cl concentration measured at the base
485 (sample SUM18-47: $0.30 \pm 0.05 \cdot 10^5$ atoms g^{-1} rock) and on the top of the modern sea
486 cliff (sample SUM18-46: $0.38 \pm 0.08 \cdot 10^5$ atoms g^{-1} rock) are an order of magnitude
487 lower than those measured on Pleistocene CRTs (I-VII) (Table 2). At the borehole site
488 (Fig. 4), the ^{36}Cl concentrations measured at the surface (C_{msurface}) and at a depth of
489 2.5 ± 0.1 m ($C_{\text{m}2.5\text{m}}$) are 6.23 ± 0.28 and $2.46 \pm 0.12 \cdot 10^5$ atoms g^{-1} rock, respectively
490 (Table 2).

491

492 **4.4. Denudation rates**

493

494 The time scales over which denudation rates are integrated (Von Blanckenburg, 2005)
495 range from 16.2 ± 0.3 (highest rate) to 237.3 ± 27.0 ka (lowest rate) with an average
496 of 61.7 ± 49.6 ka ($n = 66$). Denudation rates for the various CRTs of the sequence
497 range from 2.5 ± 0.1 to 37.1 ± 0.9 mm ka^{-1} (average at 14.7 ± 8.3 mm ka^{-1} , $n = 66$)
498 (Table 3; Fig. 6). Despite the different age hypotheses for CRT I, the denudation rates
499 calculated are more uniform than those determined for the upper CRTs (Table 3; Fig.
500 6). Denudation rates from the CRTs II₂, II₃, and II₄ are rather similar, irrespective of
501 different age hypotheses (Table 3; Fig. 6). The results suggest that cosmogenic steady

502 state has been reached for older CRTs than II₇; i.e., whatever the assigned age to the
503 CRT, the calculated denudation rates for these CRTs do not vary much (Table 3; Fig.
504 6).

505

506 The average denudation rates affecting the inner edges, main surfaces and distal
507 edges of the CRTs are 11.1 ± 7.0 (n = 16), 14.3 ± 6.8 (n = 38), and 20.8 ± 8.6 mm ka⁻¹
508 (n = 12) respectively. Denudation rates for CRTs main surfaces are widely dispersed
509 and range from 2.5 ± 0.3 (sample SUM18-37) to 29.4 ± 1.4 mm ka⁻¹ (sample SUM16-
510 8). Apart from the denudation rate calculated for sample SUM18-15 (Table 3),
511 denudation rates affecting the inner edges of CRTs I₁, II₁, II₄, II₆, V, VI are similar to
512 those of the fossil reef flats. Denudation rates for the distal edge of the CRTs are higher
513 than rates from other parts of the landform. Since the number of denudation rate values
514 is low, a non-parametric statistical test was performed (Kruskal-Wallis test) to
515 determine whether denudation rates vary significantly by morphological location of the
516 samples analyzed. The average rank of the calculated denudation rates is not
517 statistically significantly different according to the morphological location of the
518 samples ($P_{\text{value}} = 0.26$). Thus, the morphology of the CRTs does not fully explain the
519 heterogeneity of the calculated denudation rates.

520

521 Sample SUM18-46 was collected from the same surface (CRT H) of the samples used
522 for ²³⁰Th/U dating (SUM17-10 and SUM17-13) (Figs. 4; 5C). Considering ²³⁰Th/U ages
523 as the exposure time of the surface, we calculated denudation rates of 279.0 ± 0.4 mm
524 ka⁻¹ and 581.0 ± 0.4 mm ka⁻¹ (Table 3). These denudation rates (average of 430 ± 214
525 mm ka⁻¹; Table 3) near the sea level are much higher, by one to two orders of
526 magnitude, than the denudation rates calculated for the other CRTs (I-VI).

527

528 **5. Discussion**

529

530 Significant denudation rates obtained at the sea level and on the CRTs sequence point
531 to marine erosion and continental denudation as the cause of the age diachronism on
532 a single CRT (Figs. 1A; 1B). This hypothesis also requires reef reoccupation over
533 several highstands (R2 over R1 on figure 1). Our results provide the opportunity to
534 discuss the dynamics of these processes at Cape Laundi. We first highlight the role of
535 reef reoccupation processes and marine erosion in shaping CRTs. Then, we discuss
536 continental denudation by comparing our data with denudation rates published for the
537 Barbados and Puerto Rico CRTs (Lal et al., 2005), as well as for other carbonate
538 landscapes (e.g., Spencer, 1985; Vasconcelos and Stone, 2000), and focusing on the
539 variability of denudation rates.

540

541 **5.1. The genesis of the lowermost main CRT (I)**

542 **5.1.1. Reefal limestone units overlapping**

543

544 Whatever the hypothesis to explain diachronous ages on the same CRT surface, the
545 CRT internal architecture must be associated with a phenomenon of reef reoccupation
546 over several highstands in order to have recent thin reef units stacked on older units
547 (R2 over R1 in figure 1). In the borehole site of CRT 1, theoretically, if both measured
548 samples belong to the same reefal limestone unit, the ^{36}Cl concentration profile in
549 depth (constrained by an erosion rate and age) should decrease exponentially and join
550 the two measured ^{36}Cl concentration points. To construct this profile, we (1) made
551 different age hypotheses for CRT I₁, (2) used the ^{36}Cl concentration measured at the

552 surface ($C_{m_{\text{surface}}}$) to start the profile, (3) set the denudation rate automatically by
553 combining the measured ^{36}Cl concentration at the surface ($C_{m_{\text{surface}}}$) with the chosen
554 hypothetical age, and (4) set a minimum and a maximum of reef porosity from 0% (i.e.,
555 density 2.5 g cm^{-3}) to 50 % (i.e., a density of 1.25 g cm^{-3}) (e.g., Smith, 1983). We test
556 the ages proposed by Pirazzoli et al. (1991; 1993): MIS 5e, c and a, as well as an
557 extremely old age, i.e., 1.5 Ma, to test a steady state hypothesis (Schimmelpfennig et
558 al., 2009).

559

560 In any case, it is not possible to join the two ^{36}Cl concentrations measured by the
561 theoretical ^{36}Cl concentration profiles (Fig. 7). Regardless of the scenario, the 2.5 ± 0.1
562 m deep sample exhibits a ^{36}Cl concentration higher than its theoretical estimate (Fig.
563 7). The only exception is observed with a 50% porosity and the age of the drilled unit
564 estimated at 1.5 Ma. However, this age is too old compared to the dating done by
565 previous authors on the studied CRT (Pirazzoli et al., 1991; 1993; Bard et al., 1996).
566 The only way to explain the high ^{36}Cl concentration of the sample at 2.5 ± 0.1 m is that
567 this reefal limestone unit has been exposed to cosmic radiation before an overlapping
568 unit was emplaced, i.e., in a later stage of reoccupation. It follows that the borehole
569 goes through two reefal limestone units, the upper one being thinner than 2.5 m.

570

571 We thus hypothesize that this difference in the ^{36}Cl concentrations measured has been
572 acquired on the temporarily emerged surface of the CRT between two successive
573 highstands. We then calculate exposure times before overlapping with Δc (i.e.,
574 difference between the measured and theoretical ^{36}Cl concentration at a depth of 2.5
575 m; Table 4) according to possible ages of MIS 5a, MIS 5c and MIS 5e for the surface
576 unit ($Ed_{\Delta c}$ in Table 4; Pirazzoli et al., 1991; 1993; Bard et al., 1996). These values

577 correspond to minimum exposure time because after overlapping, the ^{36}Cl
578 concentration decreases with isotopic decay. Considering the ages of MIS 5e, 5c and
579 5a, which are 122 ± 6 ka, 100 ± 5 ka, and 82 ± 3 ka, respectively (Cutler et al., 2003),
580 the time intervals between isotopic stages 5e-5c, 5c-5a and 5e-5a are 22 ± 11 ka, 18
581 ± 8 ka, and 40 ± 9 ka, respectively. For the zero-porosity hypothesis, the calculated
582 exposure times before overlapping (13.8 ± 1.3 ka, 12.5 ± 1.2 ka, and 11.0 ± 1.2 ka) are
583 equivalent to the time intervals between two successive substages of MIS 5 (Table 4).
584 Consequently, our data argue that the borehole intersected two units that could be
585 associated to the two of the three relative highstands of the last interglacial: MIS 5a
586 and 5c, or MIS 5c and 5e (Table 4; Fig. 7).

587

588 We conclude that the ^{36}Cl borehole method confirms previous observations deduced
589 from $^{230}\text{Th}/\text{U}$ ages (Pirazzoli et al., 1991; 1993; Bard et al., 1996), and that CRT I₁ is
590 composite and was built during at least two successive highstands of the last
591 interglacial.

592

593 **5.1.2. Evidence for marine erosion and constructive reoccupation**

594

595 Combining cosmogenic nuclide analyses and $^{230}\text{Th}/\text{U}$ dating on reef samples collected
596 near sea level allows to discuss the hypothesis of Pirazzoli et al., (1993) that reef
597 reoccupation is associated with marine erosion (Fig. 1A). Our two samples from CRT
598 H, one at the base (SUM18-47, $0.30 \pm 0.03 \cdot 10^5$ atoms g^{-1} rock) and the other at the
599 top of the modern sea cliff (SUM18-46, $0.38 \pm 0.04 \cdot 10^5$ atoms g^{-1} rock), give similar
600 low ^{36}Cl concentrations (Table 2). If sample SUM18-47 had been recently exposed by
601 sea cliff retreat, its ^{36}Cl concentration would be much lower (e.g., Regard et al., 2012).

602 Therefore, the two samples at the top and the base of the modern sea cliff likely
603 experienced the same erosive history over the time interval resolved by the ^{36}Cl
604 method (~ 1.5 ka). In view of their location close to sea level and the high denudation
605 rates calculated from the top of the modern sea cliff (average of 430 ± 214 mm ka^{-1}),
606 the erosion process is most likely marine. The efficiency of marine erosion has already
607 been demonstrated by numerous studies, in particular using cosmonuclides (Gibb,
608 1978; Spencer, 1985; Stephenson and Kirk, 1998; Brown et al., 2003; Raimbault et al.,
609 2018). In Grand Cayman Island, the average marine erosion rate affecting reef
610 shielded coasts is 450 mm ka^{-1} (Spencer, 1985), which is in agreement with our
611 denudation rate values. However, denudation rates affecting the active sea cliff at
612 Cape Laundi were calculated on small length (sample of few centimeters) and time
613 (age hypothesis of few thousand years) scales. It may reflect the stochastic nature of
614 erosion, i.e., the detachment of a small block that can generate a large difference on
615 the calculated denudation rates. Such efficient erosion at sea level during a relatively
616 short period of time can be caused by extreme events, such as storms, cyclones, or
617 tsunamis (Anderson et al., 1999). Consequently, a comparison with denudation rates
618 averaged over much larger temporal and spatial scales may be misleading.

619

620 Whatever the uplift rate or the value of the glacial isostatic adjustment, the location of
621 the samples dated at 5.45 ± 0.02 ka and 2.13 ± 0.01 ka at the same altitude and a few
622 metres apart can only be explained by erosion and reoccupation. In addition, we have
623 observed fossil tidal pools on the CRT H surface (Fig. 5I), where the coral dated as
624 2.13 ± 0.01 ka was sampled, which allows us to specify the reoccupation mode.
625 Therefore, we interpret the coral dated at 2.13 ± 0.01 ka (SUM17-13) as a coral-colony
626 that settled on the top surface of the active sea cliff in fossil tidal pools fed by seawater

627 during high tides or storms, as observed elsewhere (e.g., Hoeksema, 2012). As such,
628 we conclude that the constructive reoccupation affected the CRT H during the Mid-
629 Holocene with a partial immersion of the reef platform.

630

631 **5.1.3. Argument of the abandonment of the main CRT (I) in a single** 632 **eustatic event.**

633

634 Cosmogenic nuclide data also inform us about the processes of CRT abandonment
635 during regression. CRT I is not old enough to have reached cosmogenic steady state.
636 However, ^{36}Cl concentrations measured on the main CRT I (I_1 , I_2) are uniform (Table
637 2, Fig. 6), suggesting a similar exposure time to radiation for the whole surface of CRT
638 I. Thus, the abandonment of CRT I surface most probably corresponds to a discrete,
639 single event, during regression after the last interglacial highstand.

640

641 **5.2. Continental denudation of CRTs**

642 **5.2.1. Comparison with global trends of carbonate denudation** 643 **rates**

644

645 In previous studies, continental denudation of reef carbonate landforms has been
646 quantified by taking direct *in situ* measurements, for example, ^{36}Cl concentrations (Lal
647 et al., 2005) as well as micro-erosion (e.g., Trudgill, 1976; 1979). Each method is
648 representative of a given period of time on which the calculated denudation rates are
649 integrated. For the ^{36}Cl method, this period is between 10^3 to 10^5 years. In contrast,
650 the micro-erosion method covers periods of only one to two years (e.g., Trudgill, 1976;
651 Spencer, 1985).

652

653 Denudation rates at Cap Laundi (average of $14.7 \pm 8.3 \text{ mm ka}^{-1}$), where precipitation
654 rates are $\sim 1000 \text{ mm a}^{-1}$, are lower than those of tropical sites with higher rainfall ($>$
655 2000 mm a^{-1}), such as in Papua New Guinea (denudation rate of $\sim 150 \text{ mm ka}^{-1}$,
656 Vasconcelos and Stone, 2000), higher than those obtained in arid to hyper-arid zones
657 (denudation rate of from 1 to 3 mm ka^{-1} , Ryb et al., 2014) and similar to those derived
658 with the same method (^{36}Cl concentration) on the same features (upper Pleistocene
659 CRTs) at locations with the same mean annual precipitation rates (1200 - 1500 mm a^{-1}
660 in Rendezvous Hill, Barbados and $\sim 915 \text{ mm a}^{-1}$ in Isla Mona, Puerto Rico). Denudation
661 rates range from 7 to 118 mm ka^{-1} on the Rendezvous Hill and from 26 to 61 mm ka^{-1}
662 at Isla Mona (Lal et al., 2005). Trudgill (1976; 1979) obtained similar denudation rates
663 (9 - 62 mm ka^{-1}) in Aldabra atoll (Seychelles archipelago), that receives comparable
664 rainfalls (Shekeine et al., 2015). Thus, denudation rates calculated at Cape Laundi are
665 consistent with the global correlation between rainfall and denudation rates determined
666 by the *in situ* ^{36}Cl method on carbonate flat surfaces (Ryb et al., 2014; Levenson et al.,
667 2017). These continental denudation rates imply a surface stripping rate of 0.7 to 2.3
668 m per glacial/interglacial cycle. If the younger reef unit are thin as suggested by the
669 drilling results, this stripping is sufficient to reveal older reef units at the surface (Fig.
670 1C).

671

672 **5.2.2. Heterogeneous variations of denudation rates across the** 673 **sequence as well as individual CRT**

674

675 Denudation rates (i.e., ^{36}Cl concentrations) vary across the sequence, as well as within
676 each CRT. In the following, we propose that this is mainly due to the sampling bias

677 related to the roughness of the carbonate surfaces and the staircase morphology of
678 the sequence.

679

680 **5.2.2.1. Roughness versus ^{36}Cl concentrations**

681

682 Over time, aerial dissolution forms larger and larger dissolution pits, amplifying the
683 roughness of the CRT (Figs. 5A; 5B; 5F; 5G). Thus, at Cape Laundi, the older the CRT,
684 the rougher it is (Figs. 5A; 5B; 5F; 5G). The roughness of all CRTs is in the order of
685 decimeters (Fig. 5B). We also observed a coastal karren-type epikarstification (e.g.,
686 Lundberg, 2019). This process induces a detachment of 10 to 50 cm thick blocks from
687 the CRT surface (Figs. 5B; 8A; 8B). The types of corals, sediments, and stage of
688 cementation produce distinctive layers of limestone rocks in fossilized reefs (James
689 and Macintyre, 1985). The layering of the paleo-reef could therefore play an important
690 role in the development of these karstic forms (Figs. 8A; 8B).

691

692 Block detachment could produce a change of ^{36}Cl concentrations over the CRTs
693 surfaces with low values on recently dismantled zones. The following goal is to get an
694 independent estimate of the typical block size removed by these karstification
695 processes using our ^{36}Cl data. We selected two pairs of surface samples from the flat
696 part of the same CRT that yield different ^{36}Cl concentrations (SUM18-21/SUM16-4 and
697 SUM18-20/SUM16-10) and we hypothesized that the difference in ^{36}Cl concentration
698 values for each pair is related to the dismantling of the surface blocks. The pairs are
699 located on CRTs I₂ and II₄, respectively (Fig. 8C). We calculate the theoretical depth
700 profile of ^{36}Cl concentrations from the CRTs age inferred by Pirazzoli et al. (1991; 1993)
701 combined with the measured ^{36}Cl concentration for the most concentrated surface

702 sample (Fig. 8C). To quantify the stripped thickness required to achieve the lowest ^{36}Cl
703 concentration of each pair, we projected this concentration onto the calculated
704 theoretical depth profile of ^{36}Cl concentrations (Fig. 8C). We obtained stripped
705 thicknesses of ~30 cm and ~82 cm for CRTs I₂ and II₄, respectively (Fig. 8C). These
706 results are consistent with the natural roughness observed and the height generated
707 by the detachment of a block (Figs. 5B; 8A). Thus, the difference in ^{36}Cl concentration
708 between each pair of samples can be attributed to the removal of a single block.
709 Variations in ^{36}Cl concentration on the same CRT can be explained by the spatial
710 variations of the degradation of the initial CRT surface. The greater the thickness of
711 the removed blocks, the greater the variations in ^{36}Cl concentration at the surface
712 related to its dismantling will be (Figs. 8B; 8C). Such spatial variations in denudation
713 rates imply that it is impossible to accurately date, with the analysis cosmogenic ^{36}Cl
714 concentrations, a CRT that has not yet reached the steady state (such as CRT I)
715 because it requires having a uniform value of this parameter all along the CRT.
716 Besides, these results suggest that on a given polycyclic CRT, the continental
717 denudation can partially strip the thin superficial layer of a young fossil coral reef and
718 exhume older corals in several places.

719

720 **5.2.2.2. CRT morphology versus ^{36}Cl concentrations**

721

722 When samples are divided according to their distribution on the CRT (i.e., inner edge,
723 terrace main surface, and distal edge) (Table 3), denudation rates reveal different
724 averages, with the highest values for the distal edges (Fig. 9). Although the non-
725 parametric statistical test (Kruskal-Wallis test) reveals that there is no significant
726 difference in denudation rates as a function of the morphological location of the sample

727 analyzed ($P_{\text{value}} = 0.26$), we consider that the distal edges are the most sensitive to
728 continental denudation because of their position at the top of the slope (Figs. 2; 6). In
729 this case, distal edges could be faster dissolved by diffusion between the fossil sea cliff
730 and fossil reef flat, and regressive erosion associated with runoff on the cliff. The flat
731 geometry of the CRT main surfaces prevents diffusion and runoff that could increase
732 the denudation rate. Furthermore, there may be a change in porosity between the main
733 surface and the distal edge of CRTs that may cause the dissolution rate to vary
734 spatially. The main surfaces of CRTs, considered a paleo lagoon (Cabioch, 2011), can
735 be then partly formed by the compaction and deposition of marine cements (Figs. 5C;
736 5D; 5E; Hopley, 2011), which reduces the porosity of the framework. The distal edges
737 of the CRTs, considered as the paleo reef crests (e.g., Pirazzoli et al., 1991; Rovere et
738 al., 2016), therefore appear to have a higher porosity than the main surfaces. The
739 greater the porosity, the more it allows the infiltration of meteoric water, accelerating
740 chemical dissolution and therefore potentially the denudation rate. Which in turn
741 explains the high roughness of the distal edges compared to other parts of the CRTs
742 (Fig. 5G).

743

744 **5.2.2.3. Water, sands cover and soil formation on CRT**

745 **versus ^{36}Cl concentration**

746

747 CRTs may be flooded during the subsequent interglacial substages if uplift rates are
748 low or if marine erosion lowers the CRT (Fig. 1). This process could play a role in
749 shielding and affect the production of ^{36}Cl on CRTs older than Holocene. However, the
750 integration time of the denudation rates calculated here (i.e., 61.7 ± 49.6 ka in average)
751 is too short to have recorded several highstands.

752

753 Besides, CRTs may also be covered by sand and debris during and after periods of
754 intense marine erosion. Indeed, we observed that CRT I₁ surface is covered by
755 centimeter-scale remnants of a sandstone layer including coral rubbles (Fig. 5E). The
756 process that forms this layer may be related to marine diagenetic cementation (Rasser
757 and Riegl, 2002). Storms are the natural events that generally explain the formation
758 and deposition of these layers (e.g., Scoffin, 1993; Bourrouilh-Le Jan, 1998; Blanchon
759 et al. 1997; Rasser and Riegl, 2002). Yet, they are also common features in sites
760 characterised by gently sloping, pre-existing surfaces (i.e., composite CRTs in our
761 study site) and medium wave energy (Cabiocch et al., 1995). These sand patches are
762 widely scattered on the lower CRTs and are absent on the upper CRTs due to
763 continental denudation. They must have been removed during the CRT emergence by
764 marine erosion (only a few pieces remain; Figs. 5C; 5E) and by continental denudation
765 after the reef emersion. With a continental denudation rate of $14.7 \pm 8.3 \text{ mm ka}^{-1}$ on
766 average, it takes only ~7000 years to strip off a few tens of centimeters. Besides, this
767 thickness is too small to significantly affect the denudation rates and to be distinguished
768 from the stripping effect.

769

770 Our field observations have shown that soil is almost non-existent on the lowest CRTs
771 (Figs. 5D; 5E) and the soil on CRTs above CRT III is very thin (a few millimeters to
772 centimeters) and only allows the formation of vegetation of steppe moor (Figs. 5A; 5B;
773 5D; 5F; 5G). The relatively dry climate of the Cape Laundi region (e.g., Prasetia et al.,
774 2013) may be the cause of the lack of thick soil, which can affect the production of ³⁶Cl.
775 But despite this arid climate, the contribution of volcanic ash from the Sunda-Banda
776 arc or of Australian dust could favour the development of soil. This has already been

777 observed in Barbados, where the parent materials of the soils on uplifted CRTs are
778 Sahara dust and volcanic ash from the Lesser Antilles Island arc (Muhs, 2001). Similar
779 examples have been reported in Taiwan (Liew and Hsieh, 2000) as well as in Liuchiu
780 Island (Cheng et al., 2011). It remains an open question whether deforestation (e.g.,
781 Orr et al, 2012) and agricultural burning (e.g., Russell-Smith et al., 2007) could have
782 removed the soil formed over time, despite the low runoff induced by the horizontality
783 of the surfaces of the CRT. We have not observed any soil trapped and preserved in
784 the dissolution features (i.e., coastal karren; Lundberg, 2019) or superficial cracks of
785 the CRTs to testify to its previous existence. Over time, soil forms from the *in situ*
786 weathering of the initial surface of the CRT and thickens. An older CRT should
787 therefore have a thicker soil, a more weathered surface and be more protected from
788 cosmic rays (shielding action) than a more recent CRT. Thus, we should have
789 observed a decrease in the ^{36}Cl concentration with the age of the CRT with former
790 thick soil now gone. We have not observed such a trend in our data. Therefore, we
791 have no evidence of the influence of soils on the ^{36}Cl production in the CRTs at Cape
792 Laundi.

793

794 **6. Conclusions**

795

796 At Cape Laundi, previous studies (Pirazzoli et al., 1991; 1993; Bard et al., 1996) have
797 identified age discrepancies on CRTs. We disentangled the roles of continental
798 denudation, coastal erosion, and marine reoccupation in the promiscuity of diachron
799 coral colonies on the same CRT surface. The ^{36}Cl concentrations of 34 surface
800 limestone samples taken from different morphological zones of this CRTs sequence
801 allowed us to calculate continental denudation rates, ranging from 2.5 ± 0.3 to $37.1 \pm$

802 0.1 mm ka⁻¹ (14.7 ± 8.3 mm ka⁻¹ on average). The combined analysis of ²³⁰Th/U ages
803 and cosmogenic ³⁶Cl concentrations of surface and depth samples in both the distal
804 and proximal part of the lowermost CRT suggest that this CRT is composite and
805 records a polycyclic history with alternating construction and erosion phases during the
806 eustatic sea level variations of the last interglacial highstands (MIS 5e, 5c, and 5a) and
807 during the Mid-Holocene. Our results also highlight 1) significant spatial variability in
808 denudation rates, probably related to roughness and morphological zoning of CRTs,
809 which could bring coral colonies of different ages to the surface depending on the
810 efficiency of continental denudation, and 2) higher denudation rates affecting the distal
811 edges of CRTs than in other parts of the landform. Eventually, we stress that such
812 erosion processes, suggested since a long time but rarely discussed in the literature,
813 should be systematically taken into account when establishing the morphostratigraphy
814 of emerged coral reef terrace sequences.

815

816 **Acknowledgements**

817

818 This work was supported by public funds received of the program "Investissements
819 d'Avenir" managed by the French National Research Agency (ANR-10-EQPX-20 and
820 ANR-10-LABX-19-01, Labex Mer, CLIMORESO, C. Authemayou), the INSU Tellus
821 Syter program (SECOMAS, C. Authemayou), and the CNES TOSCA program
822 (CETTROPICO, C. Authemayou). We thank the German Aerospace Center for
823 providing us the TanDEM-X data for our study zone. We thank the State Ministry of
824 Research and Technology of Indonesia "RISTEK" that allowed us to conduct the field
825 trip to Sumba (research permit 680/FRP/E5/Dit.KI/IV/2017). We also thank the
826 National Geographic Explorer grant (no CP 087R 17) to support the Indonesian

827 researchers (Sri Yudawati Cahyarini, Vera Christanti Agusta, and Danny Hilman
828 Natawidjaja). Denis Scholz is thankful to the DFG for funding (SCHO 1274/11e1 and
829 INST 247/889-1 FUGG). We thank Gilles Brocard for his help with karstic terminology.
830 Finally, we thank 3 anonymous reviewers for fruitful discussions on former versions of
831 this manuscript.

832

833 **References cited**

834

- 835 **1.** Abdullah, C. I., Rampnoux, J. P., Bellon, H., Maury, R. C., & Soeria-Atmadja, R.
836 **(2000)**. The evolution of Sumba Island (Indonesia) revisited in the light of new
837 data on the geochronology and geochemistry of the magmatic rocks. *Journal of*
838 *Asian Earth Sciences*, 18(5), 533-546.
- 839
- 840 **2.** Alfonso-Sosa, E. **(2016)**. Tidal mixing in the Sumba Strait and internal wave
841 activity detected during strong semidiurnal forcing.
- 842
- 843 **3.** Andersen, M. B., Stirling, C. H., Zimmermann, B., & Halliday, A. N. **(2010)**.
844 Precise determination of the open ocean $^{234}\text{U}/^{238}\text{U}$ composition.
845 *Geochemistry, Geophysics, Geosystems*, 11(12).
- 846
- 847 **4.** Anderson, R. S., Densmore, A. L., & Ellis, M. A. **(1999)**. The generation and
848 degradation of marine terraces. *Basin Research*, 11(1), 7-20.
- 849
- 850 **5.** Authemayou, C., Brocard, G., Delcaillau, B., Molliex, S. p., Pedoja, K., Husson,
851 L., et al. **(2018)**. Unraveling the roles of asymmetric uplift, normal faulting and

852 groundwater flow to drainage rearrangement in an emerging karstic landscape.
853 Earth Surface Processes and Landforms, 43(9), 1885-1898.
854

855 **6.** Bard, E., Jouannic, C., Hamelin, B., Pirazzoli, P., Arnold, M., Faure, G., et al.
856 (1996). Pleistocene sea levels and tectonic uplift based on dating of corals from
857 Sumba Island, Indonesia. Geophysical Research Letters, 23(12), 1473-1476.
858

859 **7.** Bierman, P. R. (1994). Using in situ produced cosmogenic isotopes to estimate
860 rates of landscape evolution: A review from the geomorphic perspective.
861 Journal of Geophysical Research: Solid Earth, 99(B7), 13885-13896.
862

863 **8.** Blanchon, P., Jones, B., & Kalbfleisch, W. (1997). Anatomy of a fringing reef
864 around Grand Cayman; storm rubble, not coral framework. Journal of
865 Sedimentary Research, 67(1), 1-16.
866

867 **9.** Bourrouilh-Le Jan, F. G. (1998). The role of high-energy events (hurricanes
868 and/or tsunamis) in the sedimentation, diagenesis and karst initiation of tropical
869 shallow water carbonate platforms and atolls. Sedimentary Geology, 118(1-4),
870 3-36.
871

872 **10.** Braucher, R., Del Castillo, P., Siame, L., Hidy, A. J., & Bourles, D. L. (2009).
873 Determination of both exposure time and denudation rate from an in situ-
874 produced ¹⁰Be depth profile: a mathematical proof of uniqueness. Model
875 sensitivity and applications to natural cases. Quaternary Geochronology, 4(1),
876 56-67.

877

878 **11.**Braucher, R., Merchel, S., Borgomano, J., & Bourlès, D. L. (2011). Production
879 of cosmogenic radionuclides at great depth: a multi element approach. Earth
880 and Planetary Science Letters, 309(1-2), 1-9.

881

882 **12.**Brown, J., Jorgenson, M. T., Smith, O. P., & Lee, W. (2003). Long-term rates of
883 coastal erosion and carbon input, Elson Lagoon, Barrow, Alaska. Paper
884 presented at the Eighth International Conference on Permafrost.

885

886 **13.**Butt, T., Russell, P., & Grigg, R. (2004). Surf science: An introduction to waves
887 for surfing: University of Hawaii Press Honolulu.

888

889 **14.**Cabioch, G., Montaggioni, L. F., & Faure, G. (1995). Holocene initiation and
890 development of New Caledonian fringing reefs, SW Pacific. Coral Reefs, 14(3),
891 131-140.

892

893 **15.**Cabioch, G. (2011). Emerged reefs. Encyclopedia of Modern Coral Reefs:
894 Structure, Form and Process, 373-380.

895

896 **16.**Chappell, J. (1974). Geology of coral terraces, Huon Peninsula, New Guinea: a
897 study of Quaternary tectonic movements and sea-level changes. Geological
898 Society of America Bulletin, 85(4), 553-570.

899

900 **17.**Cheng, C.-H., Jien, S.-H., Tsai, H., & Hseu, Z.-Y. (2011). Geomorphological and
901 paleoclimatic implications of soil development from siliceous materials on the

902 coral-reef terraces of Liuchiu Island in southern Taiwan. Soil science and plant
903 nutrition, 57(1), 114-127.

904

905 **18.**Codilean, A. T. (2006). Calculation of the cosmogenic nuclide production
906 topographic shielding scaling factor for large areas using DEMs. Earth Surface
907 Processes and Landforms, 31(6), 785-794.

908

909 **19.**Colas, A., & Sutherland, B. (2001). The world stormrider guide: Low Pressure.

910

911 **20.**Crosby, W. O. (1883). Elevated coral reefs of cuba. Journal of Natural History,
912 12(70), 283-284.

913

914 **21.**Cutler, K. B., Edwards, R. L., Taylor, F. W., Cheng, H., Adkins, J., Gallup, C. D.,
915 et al. (2003). Rapid sea-level fall and deep-ocean temperature change since the
916 last interglacial period. Earth and Planetary Science Letters, 206(3-4), 253-271.

917

918 **22.**Daly, R. A. (1915). The glacial-control theory of coral reefs.

919

920 **23.**Darwin, C. (1842). The Structure and Distribution of Coral Reefs: Being the First
921 Part of the Geology of the Voyage of the Beagle... During the Years 1832-1836:
922 Smith, Elder.

923

924 **24.**Dunai, T. J. (2010). Cosmogenic Nuclides: Principles, concepts and
925 applications in the Earth surface sciences: Cambridge University Press.

926

- 927 **25.** Fabryka-Martin, J. T. (1988). Production of radionuclides in the earth and their
928 hydrogeologic significance, with emphasis on chlorine-36 and iodine-129.
929
- 930 **26.** Fleury, J.-M., Pubellier, M., & de Urreiztieta, M. (2009). Structural expression of
931 forearc crust uplift due to subducting asperity. *Lithos*, 113(1-2), 318-330.
932
- 933 **27.** Fortuin, A. R., Van der Werff, W., & Wensink, H. (1997). Neogene basin history
934 and paleomagnetism of a rifted and inverted forearc region, on-and offshore
935 Sumba, Eastern Indonesia. *Journal of Asian Earth Sciences*, 15(1), 61-88.
936
- 937 **28.** Granger, D. E., & Riebe, C. S. (2014). Cosmogenic nuclides in weathering and
938 erosion.
939
- 940 **29.** Gibb, J. G. (1978). Rates of coastal erosion and accretion in New Zealand. *New
941 Zealand journal of marine and freshwater research*, 12(4), 429-456.
942
- 943 **30.** Gosse, J. C., & Phillips, F. M. (2001). Terrestrial in situ cosmogenic nuclides:
944 theory and application. *Quaternary Science Reviews*, 20(14), 1475-1560.
945
- 946 **31.** Haig, D. W. (2012). Palaeobathymetric gradients across Timor during 5.7-3.3
947 Ma (latest Miocene-Pliocene) and implications for collision uplift.
948 *Palaeogeography, Palaeoclimatology, Palaeoecology*, 331, 50-59.
949

- 950 **32.**Hantoro, W. S., Jouannic, C., & Pirazzoli, P. A. (1989). Terrasses coralliennes
951 quaternaires soulevées dans l'île de Sumba (Indonésie). Photo interprétation
952 (Paris), 28(1), 17-34.
- 953
- 954 **33.**Hantoro, W. S. (1992). Etude des terrasses récifales Quaternaires soulevées
955 entre le Détroit de la Sonde et l'île de Timor, Indonésie: mouvements verticaux
956 de la croûte terrestre et variations du niveau de la mer.
- 957
- 958 **34.**Harris, R. A. (1991). Temporal distribution of strain in the active Banda orogen:
959 a reconciliation of rival hypotheses. Journal of Southeast Asian Earth Sciences,
960 6(3-4), 373-386.
- 961
- 962 **35.**Hearty, P. J., & Olson, S. L. (2008). Mega-highstand or megatsunami?
963 Discussion of McMurtry et al. (Elevated marine deposits in Bermuda record a
964 late Quaternary megatsunami: Sed. Geol. 200 (2007) 155-165). Sedimentary
965 Geology, 203(3-4), 307-312.
- 966
- 967 **36.**Hein, A. S., Hulton, N. R. J., Dunai, T. J., Schnabel, C., Kaplan, M. R., Naylor,
968 M., et al. (2009). Middle Pleistocene glaciation in Patagonia dated by
969 cosmogenic-nuclide measurements on outwash gravels. Earth and Planetary
970 Science Letters, 286(1-2), 184-197.
- 971
- 972 **37.**Heisinger, B., Lal, D., Jull, A. J. T., Kubik, P., Ivy-Ochs, S., Neumaier, S., et al.
973 (2002). Production of selected cosmogenic radionuclides by muons: 1. Fast
974 muons. Earth and Planetary Science Letters, 200(3-4), 345-355.

975
976
977
978
979
980
981
982
983
984
985
986
987
988
989
990
991
992
993
994
995
996
997
998
999

- 38.**Hibbert, F. D., Rohling, E. J., Dutton, A., Williams, F. H., Chutcharavan, P. M., Zhao, C., et al. (2016). Coral indicators of past sea-level change: A global repository of U-series dated benchmarks. *Quaternary Science Reviews*, 145, 1-56.
- 39.**Hinschberger, F., Malod, J.-A., Réhault, J.-P., Villeneuve, M., Royer, J.-Y., & Burhanuddin, S. (2005). Late Cenozoic geodynamic evolution of eastern Indonesia. *Tectonophysics*, 404(1-2), 91-118.
- 40.**Hoeksema, B. W. (2012). Extreme morphological plasticity enables a free mode of life in *Favia gravida* at Ascension Island (South Atlantic). *Marine Biodiversity*, 42(2), 289-295.
- 41.**Hopley, D. (2011). Density and porosity: influence on reef accretion rates. In: Springer.
- 42.**Husson, L., Pastier, A.-M., Pedoja, K., Elliot, M., Paillard, D., Authemayou, C., et al. (2018). Reef carbonate productivity during Quaternary sea level oscillations. *Geochemistry, Geophysics, Geosystems*, pp. 1148-1164.
- 43.**James, N. P., & Macintyre, I. G. (1985). Carbonate depositional environments- modern and ancient-Part. 1: Reefs-zonation, depositional facies and diagenesis. *Colorado School of Mines Quarterly*, 80(3).

- 1000 **44.**Jouannic, C., Hantoro, W. S., Hoang, C. T., Fournier, M., Lafont, R., & Ichtam,
1001 M. L. (1988). Quaternary raised reef terraces at cape Laundi, Sumba,
1002 Indonesia: geomorphological analysis and first radiometric Th/U and ¹⁴C age
1003 determinations. Paper presented at the 6th Proceedings International coral reef
1004 symposium.
- 1005
- 1006 **45.**Kindler, P., Reyss, J.-L., Cazala, C., & Plagnes, V. r. (2007). Discovery of a
1007 composite reefal terrace of middle and late Pleistocene age in Great Inagua
1008 Island, Bahamas. Implications for regional tectonics and sea-level history.
1009 *Sedimentary Geology*, 194(1-2), 141-147.
- 1010
- 1011 **46.**Kummerow, C., Simpson, J., Thiele, O., Barnes, W., Chang, A. T. C., Stocker,
1012 E., et al. (2000). The status of the Tropical Rainfall Measuring Mission (TRMM)
1013 after two years in orbit. *Journal of applied meteorology*, 39(12), 1965-1982.
- 1014
- 1015 **47.**Lal, D. (1988). In situ-produced cosmogenic isotopes in terrestrial rocks. *Annual*
1016 *Review of Earth and Planetary Sciences*, 16(1), 355-388.
- 1017
- 1018 **48.**Lal, D. (1991). Cosmic ray labeling of erosion surfaces: in situ nuclide production
1019 rates and erosion models. *Earth and Planetary Science Letters*, 104(2-4), 424-
1020 439.
- 1021
- 1022 **49.**Lal, D., Gallup, C. D., Somayajulu, B. L. K., Vacher, L. c., Caffee, M. W., Jull, A.
1023 J. T., et al. (2005). Records of cosmogenic radionuclides ¹⁰Be, ²⁶Al and ³⁶Cl

1024 in corals: First studies on coral erosion rates and potential of dating very old
1025 corals. *Geochimica et cosmochimica acta*, 69(24), 5717-5728.

1026

1027 **50.**Levenson, Y., Ryb, U., & Emmanuel, S. (2017). Comparison of field and
1028 laboratory weathering rates in carbonate rocks from an Eastern Mediterranean
1029 drainage basin. *Earth and Planetary Science Letters*, 465, 176-183.

1030

1031 **51.**Liew, P.-M., & Hsieh, M.-L. (2000). Late Holocene (2 ka) sea level, river
1032 discharge and climate interrelationship in the Taiwan region. *Journal of Asian*
1033 *Earth Sciences*, 18(4), 499-505.

1034

1035 **52.**Lundberg, J. (2019). Karren, surface. In *Encyclopedia of Caves* (pp. 600-608):
1036 Elsevier.

1037

1038 **53.**Merchel, S., Arnold, M., Aumaître, G., Benedetti, L., Bourlès, D. L., Braucher,
1039 R., et al. (2008). Towards more precise ^{10}Be and ^{36}Cl data from measurements
1040 at the 10-14 level: influence of sample preparation. *Nuclear instruments and*
1041 *methods in physics research section B: beam interactions with materials and*
1042 *atoms*, 266(22), 4921-4926.

1043

1044 **54.**Muhs, D. R. (2001). Evolution of soils on Quaternary reef terraces of Barbados,
1045 West Indies. *Quaternary research*, 56(1), 66-78.

1046

1047 **55.**Murray-Wallace, C. V., & Woodroffe, C. D. (2014). *Quaternary sea-level*
1048 *changes: a global perspective*: Cambridge University Press.

1049

1050 **56.**Nexer, M., Authemayou, C., Schildgen, T., Hantoro, W. S., Molliex, S.,
1051 Delcaillau, B., et al. (2015). Evaluation of morphometric proxies for uplift on
1052 sequences of coral reef terraces: A case study from Sumba Island (Indonesia).
1053 *Geomorphology*, 241, 145-159.

1054

1055 **57.**Nugroho, H., Harris, R., Lestariya, A. W., & Maruf, B. (2009). Plate boundary
1056 reorganization in the active Banda Arc-continent collision: Insights from new
1057 GPS measurements. *Tectonophysics*, 479(1-2), 52-65.

1058

1059 **58.**Obert, J. C., Scholz, D., Felis, T., Brocas, W. M., Jochum, K. P., & Andreae, M.
1060 O. (2016). $^{230}\text{Th}/\text{U}$ dating of Last Interglacial brain corals from Bonaire
1061 (southern Caribbean) using bulk and theca wall material. *Geochimica et*
1062 *cosmochimica acta*, 178, 20-40.

1063

1064 **59.**Obert, J. C., Scholz, D., Felis, T., Lippold, J., Jochum, K. P., & Andreae, M. O.
1065 (2019). Improved constraints on open-system processes in fossil reef corals by
1066 combined Th/U, Pa/U and Ra/Th dating: A case study from Aqaba, Jordan.
1067 *Geochimica et cosmochimica acta*, 245, 459-478.

1068

1069 **60.** Orr, Y., Schimmer, R., Geerken, R., Castro, A., Taylor, D., & Brokensha, D.
1070 (2012). Ethno-ecology in the shadow of rain and the light of experience: local
1071 perceptions of drought and climate change in east Sumba, Indonesia. *Climate*
1072 *Change and Threatened Communities* [Castro, AP, D. Taylor, and DW
1073 Brokensha (eds.)]. Practical Action Publishing, Rugby, UK, 175-184.

1074
1075
1076
1077
1078
1079
1080
1081
1082
1083
1084
1085
1086
1087
1088
1089
1090
1091
1092
1093
1094
1095
1096
1097

- 61.** Pastier, A. M., Husson, L., Pedoja, K., Bézos, A., Authemayou, C., Arias-Ruiz, C., et al. (2019). Genesis and Architecture of Sequences of Quaternary Coral Reef Terraces: Insights From Numerical Models. *Geochemistry, Geophysics, Geosystems*.
- 62.** Pedoja, K., Husson, L., Regard, V., Cobbold, P. R., Ostanciaux, E., Johnson, M. E., et al. (2011). Relative sea-level fall since the last interglacial stage: are coasts uplifting worldwide? *Earth-Science Reviews*, 108(1-2), 1-15.
- 63.** Pedoja, K., Husson, L., Johnson, M. E., Melnick, D., Witt, C., Pochat, S. p., et al. (2014). Coastal staircase sequences reflecting sea-level oscillations and tectonic uplift during the Quaternary and Neogene. *Earth-Science Reviews*, 132, 13-38.
- 64.** Pedoja, K., Husson, L., Bézos, A., Pastier, A.-M., Imran, A. M., Arias-Ruiz, C., et al. (2018). On the long-lasting sequences of coral reef terraces from SE Sulawesi (Indonesia): Distribution, formation, and global significance. *Quaternary Science Reviews*, 188, 37-57.
- 65.** Phillips, F. M., & Plummer, M. A. (1996). CHLOE; a program for interpreting in-situ cosmogenic nuclide data for surface exposure dating and erosion studies. *Radiocarbon*, 38(1), 98-99.

- 1098 **66.**Phillips, F. M., Stone, W. D., & Fabryka-Martin, J. T. (**2001**). An improved
1099 approach to calculating low-energy cosmic-ray neutron fluxes near the
1100 land/atmosphere interface. *Chemical Geology*, 175(3-4), 689-701.
1101
- 1102 **67.**Pirazzoli, P. A., Radtke, U., Hantoro, W. S., Jouannic, C., Hoang, C. T., Causse,
1103 C., et al. (**1991**). Quaternary raised coral-reef terraces on Sumba Island,
1104 Indonesia. *Science*, 252(5014), 1834-1836.
1105
- 1106 **68.**Pirazzoli, P. A., Radtke, U., Hantoro, W. S., Jouannic, C., Hoang, C. T., Causse,
1107 C., et al. (**1993**). A one million-year-long sequence of marine terraces on Sumba
1108 Island, Indonesia. *Marine Geology*, 109(3-4), 221-236.
1109
- 1110 **69.**Pirazzoli, P. A. (**2005**). A review of possible eustatic, isostatic and tectonic
1111 contributions in eight late-Holocene relative sea-level histories from the
1112 Mediterranean area. *Quaternary Science Reviews*, 24(18-19), 1989-2001.
1113
- 1114 **70.**Prasetia, R., As-syakur, A. R., & Osawa, T. (**2013**). Validation of TRMM
1115 Precipitation Radar satellite data over Indonesian region. *Theoretical and*
1116 *applied climatology*, 112(3-4), 575-587.
1117
- 1118 **71.**Raimbault, C., Duperret, A., Regard, V., Molliex, S., Wyns, R., Authemayou, C.,
1119 et al. (**2018**). Quaternary geomorphological evolution of a granitic shore platform
1120 constrained by in situ ¹⁰Be concentrations, Penmarc'h, SW Brittany, France.
1121 *Marine Geology*, 395, 33-47.
1122

- 1123 **72.**Rasser, M., & Riegl, B. (2002). Holocene coral reef rubble and its binding
1124 agents. *Coral Reefs*, 21(1), 57-72.
1125
- 1126 **73.**Regard, V., Dewez, T., Bourles, D. L., Anderson, R. S., Duperret, A., Costa, S.,
1127 et al. (2012). Late Holocene seacliff retreat recorded by ¹⁰Be profiles across a
1128 coastal platform: Theory and example from the English Channel. *Quaternary*
1129 *Geochronology*, 11, 87-97.
1130
- 1131 **74.**Rovere, A., Raymo, M. E., Vacchi, M., Lorscheid, T., Stocchi, P., Gomez-Pujol,
1132 L., et al. (2016). The analysis of Last Interglacial (MIS 5e) relative sea-level
1133 indicators: Reconstructing sea-level in a warmer world. *Earth-Science Reviews*,
1134 159, 404-427.
1135
- 1136 **75.**Rupnik, E., Deseilligny, M. P., Delorme, A., & Klinger, Y. (2016). Refined
1137 satellite image orientation in the free open-source photogrammetric tools
1138 Apero/Micmac. *ISPRS Annals of the Photogrammetry, Remote Sensing and*
1139 *Spatial Information Sciences*, 3, 83.
1140
- 1141 **76.**Russell-Smith, J., Djoeroemana, S., Maan, J., & Pandanga, P. (2007). Rural
1142 livelihoods and burning practices in savanna landscapes of Nusa Tenggara
1143 Timur, eastern Indonesia. *Human Ecology*, 35(3), 345-359.
1144
- 1145 **77.**Ryb, U., Matmon, A., Erel, Y., Haviv, I., Benedetti, L., & Hidy, A. J. (2014). Styles
1146 and rates of long-term denudation in carbonate terrains under a Mediterranean

1147 to hyper-arid climatic gradient. *Earth and Planetary Science Letters*, 406, 142-
1148 152.

1149

1150 **78.** Schaller, M., Ehlers, T. A., Blum, J. D., & Kallenberg, M. A. (2009). Quantifying
1151 glacial moraine age, denudation, and soil mixing with cosmogenic nuclide depth
1152 profiles. *Journal of Geophysical Research: Earth Surface*, 114(F1).

1153

1154 **79.** Schimmelpfennig, I., Benedetti, L., Finkel, R., Pik, R. I., Blard, P.-H., Bourles,
1155 D., et al. (2009). Sources of in-situ ^{36}Cl in basaltic rocks. Implications for
1156 calibration of production rates. *Quaternary Geochronology*, 4(6), 441-461.

1157

1158 **80.** Schimmelpfennig, I., Benedetti, L., Garreta, V., Pik, R., Blard, P.-H., Burnard,
1159 P., et al. (2011). Calibration of cosmogenic ^{36}Cl production rates from Ca and
1160 K spallation in lava flows from Mt. Etna (38 N, Italy) and Payun Matru (36 S,
1161 Argentina). *Geochimica et cosmochimica acta*, 75(10), 2611-2632.

1162

1163 **81.** Schimmelpfennig, I., Schaefer, J. M., Putnam, A. E., Koffman, T., Benedetti, L.,
1164 Ivy-Ochs, S., et al. (2014). ^{36}Cl production rate from K-spallation in the
1165 European Alps (Chironico landslide, Switzerland). *Journal of Quaternary*
1166 *Science*, 29(5), 407-413.

1167

1168 **82.** Schlagenhauf, A., Gaudemer, Y., Benedetti, L., Manighetti, I., Palumbo, L.,
1169 Schimmelpfennig, I., et al. (2010). Using in situ Chlorine-36 cosmonuclide to
1170 recover past earthquake histories on limestone normal fault scarps: a

1171 reappraisal of methodology and interpretations. *Geophysical Journal*
1172 *International*, 182(1), 36-72.

1173

1174 **83.** Scholz, D., Mangini, A., & Felis, T. (2004). U-series dating of diagenetically
1175 altered fossil reef corals. *Earth and Planetary Science Letters*, 218(1-2), 163-
1176 178.

1177

1178 **84.** Schwartz, M. (2006). *Encyclopedia of coastal science*: Springer Science &
1179 Business Media.

1180

1181 **85.** Scoffin, T. P. (1993). The geological effects of hurricanes on coral reefs and the
1182 interpretation of storm deposits. *Coral Reefs*, 12(3-4), 203-221.

1183

1184 **86.** Shekeine, J., Turnbull, L. A., Cherubini, P., de Jong, R., Baxter, R., Hansen, D.,
1185 et al. (2015). Primary productivity and its correlation with rainfall on Aldabra
1186 Atoll. *Biogeosciences Discussions*, 12(2), 981-1013.

1187

1188 **87.** Simms, A. R. (2021). Last interglacial sea levels within the Gulf of Mexico and
1189 northwestern Caribbean Sea. *Earth System Science Data*, 13(3), 1419-1439.

1190

1191 **88.** Smith, S. V. (1983). Coral reef calcification. *Perspectives on Coral Reefs*.
1192 Australian Institute of Marine Science, 240-247.

1193

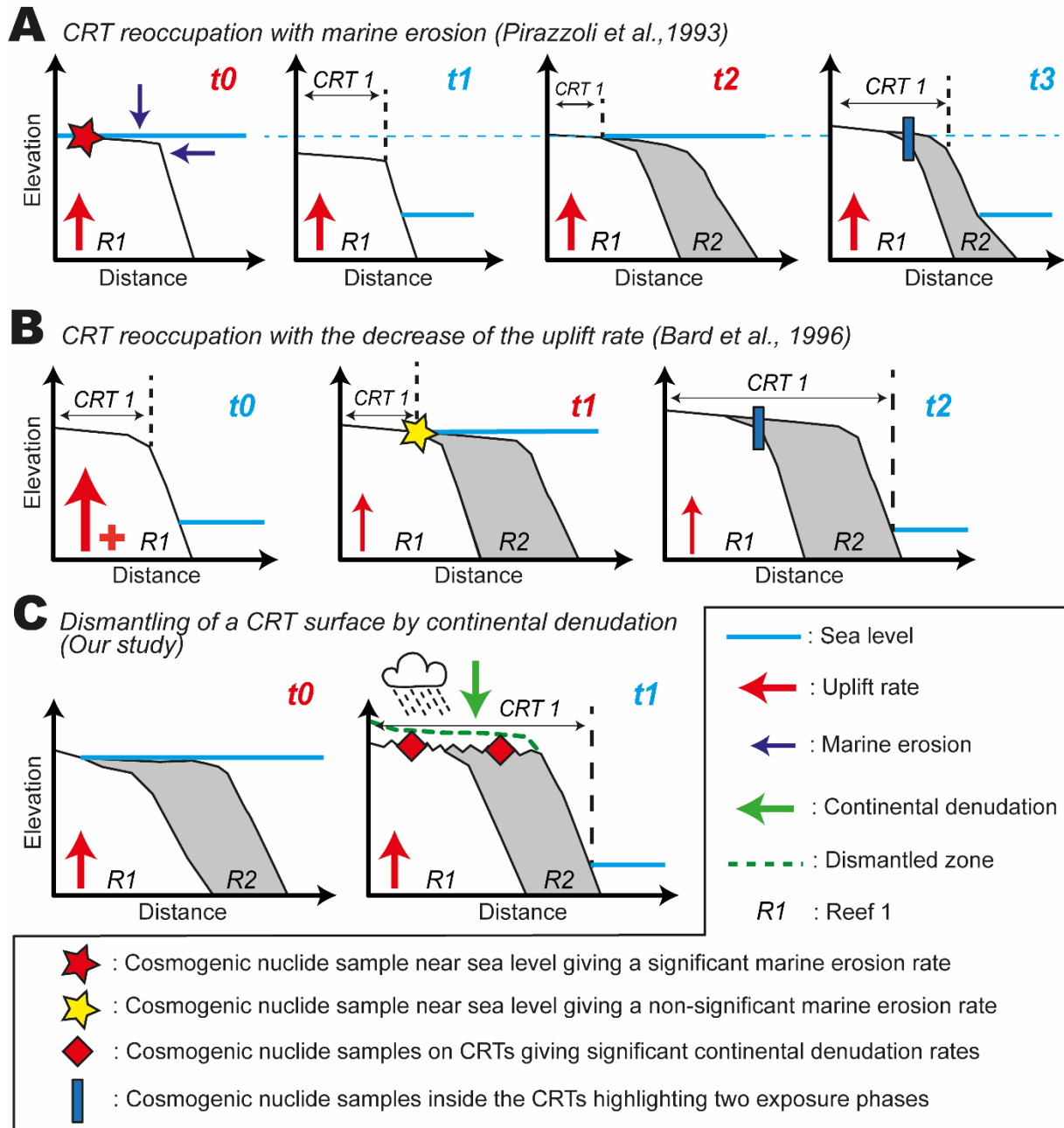
- 1194 **89.**Speed, R. C., & Cheng, H. (2004). Evolution of marine terraces and sea level in
1195 the last interglacial, Cave Hill, Barbados. *Geological Society of America Bulletin*,
1196 116(1-2), 219-232.
- 1197
- 1198 **90.**Spencer, T. (1985). Weathering rates on a Caribbean reef limestone: results
1199 and implications. *Marine Geology*, 69(1-2), 195-201.
- 1200
- 1201 **91.**Stephenson, W. J., & Kirk, R. M. (1998). Rates and patterns of erosion on inter-
1202 tidal shore platforms, Kaikoura Peninsula, South Island, New Zealand. *Earth*
1203 *Surface Processes and Landforms: The Journal of the British Geomorphological*
1204 *Group*, 23(12), 1071-1085.
- 1205
- 1206 **92.**Stone, J., Allan, G. L., Fifield, L. K., Evans, J. M., & Chivas, A. R. (1994).
1207 Limestone erosion measurements with cosmogenic chlorine-36 in calcite-
1208 preliminary results from Australia. *Nuclear instruments and methods in physics*
1209 *research section B: beam interactions with materials and atoms*, 92(1-4), 311-
1210 316
- 1211
- 1212 **93.**Stone, J. O., Allan, G. L., Fifield, L. K., & Cresswell, R. G. (1996). Cosmogenic
1213 chlorine-36 from calcium spallation. *Geochimica et cosmochimica acta*, 60(4),
1214 679-692.
- 1215
- 1216 **94.**Stone, J. O. H., Evans, J. M., Fifield, L. K., Allan, G. L., & Cresswell, R. G.
1217 (1998). Cosmogenic chlorine-36 production in calcite by muons. *Geochimica et*
1218 *cosmochimica acta*, 62(3), 433-454.

1219
1220
1221
1222
1223
1224
1225
1226
1227
1228
1229
1230
1231
1232
1233
1234
1235
1236
1237
1238
1239
1240
1241
1242

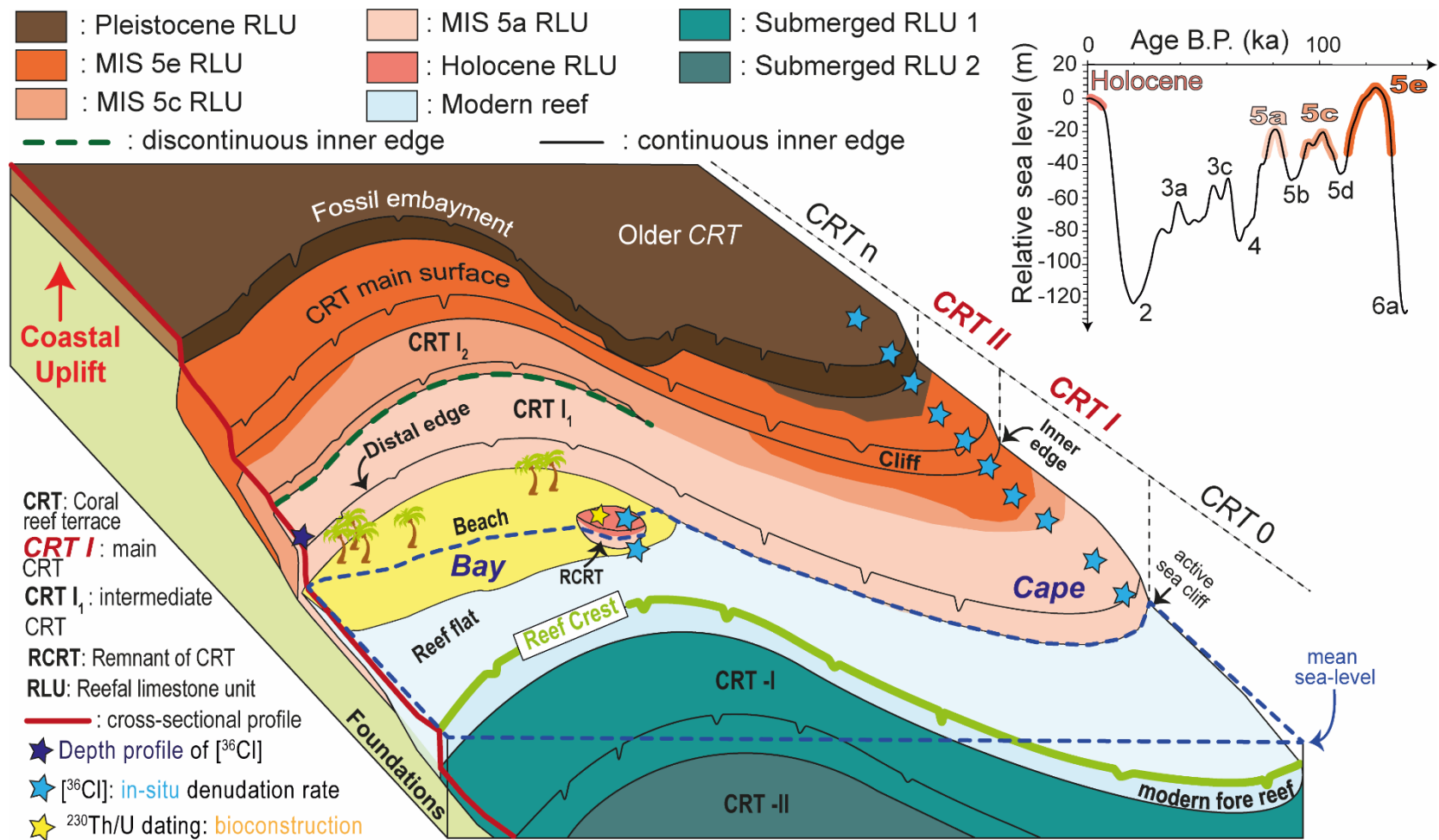
- 95.** Tate, G. W., McQuarrie, N., Van Hinsbergen, D. J. J., Bakker, R. R., Harris, R., Willett, S., et al. (2014). Resolving spatial heterogeneities in exhumation and surface uplift in Timor-Leste: Constraints on deformation processes in young orogens. *Tectonics*, 33(6), 1089-1112.
- 96.** Thompson, S. B., & Creveling, J. R. (2021). A Global Database of Marine Isotope Stage 5a and 5c Marine Terraces and Paleoshoreline Indicators. *Earth System Science Data Discussions*, 1-32.
- 97.** Trudgill, S. T. (1976). The marine erosion of limestones on Aldabra Atoll, Indian Ocean. *Zeitschrift für Geomorphologie*, 26, 164-200.
- 98.** Trudgill, S. T. (1979). Surface lowering and landform evolution on Aldabra. *Philosophical Transactions of the Royal Society of London. B, Biological Sciences*, 286(1011), 35-45.
- 99.** Van der Werff, W. (1995). Cenozoic evolution of the Savu Basin, Indonesia: forearc basin response to arc-continent collision. *Marine and Petroleum Geology*, 12(3), 247-262.
- 100.** Vasconcelos, P. M. D., & Stone, J. O. (2000). Studies of geomorphic rates and processes with cosmogenic isotopes-examples from Australia.

- 1243 **101.** Vermeesch, P. (2007). CosmoCalc: An Excel add-in for cosmogenic
1244 nuclide calculations. *Geochemistry, Geophysics, Geosystems*, 8(8).
1245
- 1246 **102.** Von Blanckenburg, F. (2005). The control mechanisms of erosion and
1247 weathering at basin scale from cosmogenic nuclides in river sediment. *Earth
1248 and Planetary Science Letters*, 242(3-4), 224-239.
1249
- 1250 **103.** Von der Borch, C. C., Grady, A. E., Hardjoprawiro, S., Prasetyo, H., &
1251 Hadiwisastra, S. (1983). Mesozoic and late Tertiary submarine fan sequences
1252 and their tectonic significance, Sumba, Indonesia. *Sedimentary Geology*, 37(1-
1253 2), 113-132.
1254
- 1255 **104.** Waelbroeck, C., Labeyrie, L., Michel, E., Duplessy, J. C., McManus, J.
1256 F., Lambeck, K., et al. (2002). Sea-level and deep water temperature changes
1257 derived from benthic foraminifera isotopic records. *Quaternary Science
1258 Reviews*, 21(1-3), 295-305.
1259
- 1260 **105.** Yang, Q., Scholz, D., Jochum, K. P., Hoffmann, D. L., Stoll, B., Weis, U.,
1261 et al. (2015). Lead isotope variability in speleothems-A promising new proxy for
1262 hydrological change? First results from a stalagmite from western Germany.
1263 *Chemical Geology*, 396, 143-151.
1264
1265
1266

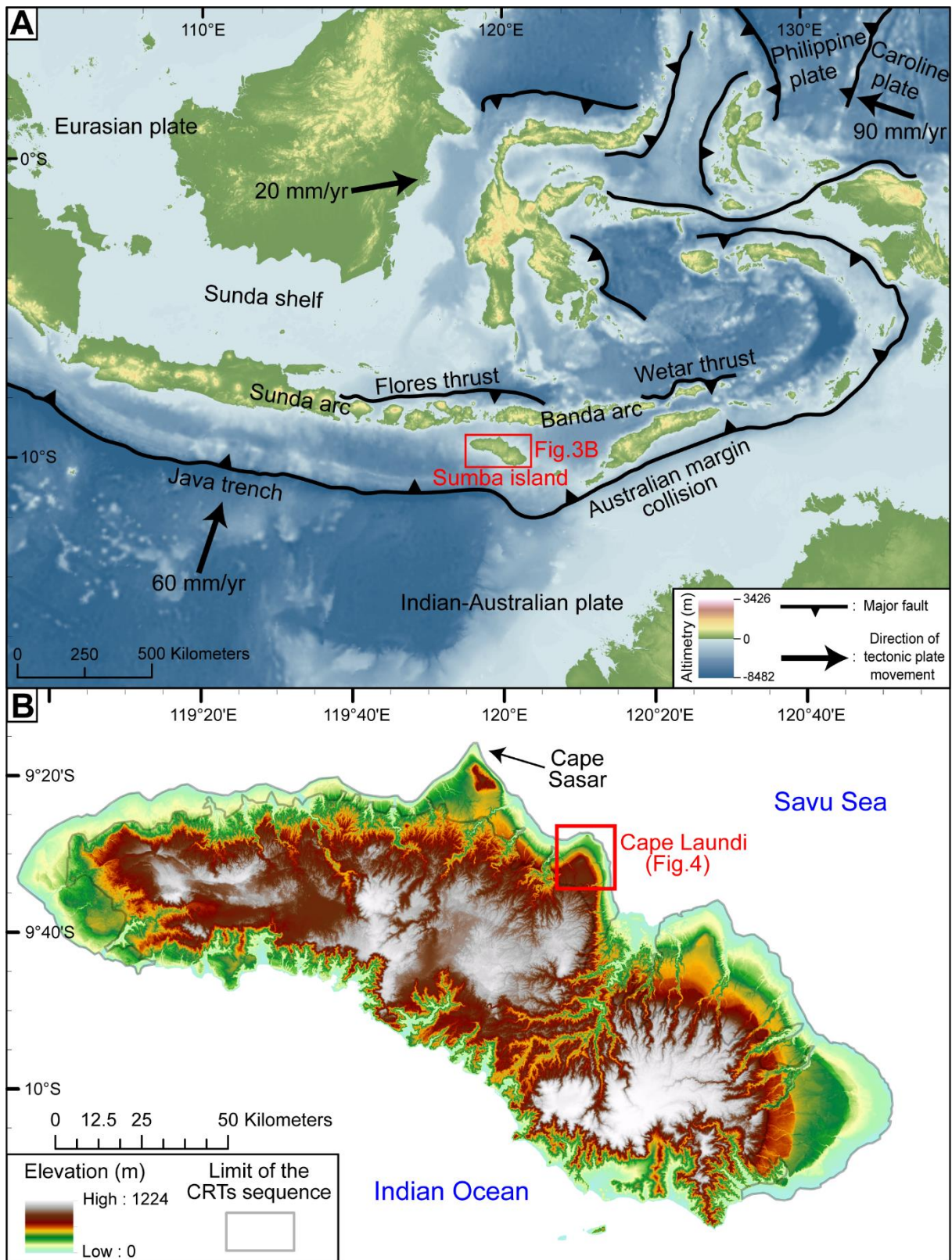
Figures



1269 **Fig. 1.** Three hypotheses explaining diachronous ages on the same surface of the
1270 Cape Laundi CRTs. **A)** Important role of marine erosion in the destruction of the
1271 emergent CRTs, helping a later reoccupation of these eroded surfaces (Pirazzoli et al.,
1272 1993). **B)** The decrease in the rate of uplift to a low rate (about 0.2 mm a^{-1}) promotes
1273 the reoccupation of emergent CRTs without marine erosion (Bard et al., 1996). **C)**
1274 Alternative hypothesis (this study): continental denudation may partially dismantle
1275 emergent surfaces, generating a diachronism of these surfaces. ^{36}Cl cosmogenic
1276 data on CRT near current sea level reveal the significance of marine erosion (Fig. 1A)
1277 and continental denudation (Fig. 1C).



1278 **Fig. 2.** Schematic plot of a sequence of coral reef terraces, modified from Pedoja et al. (2018). The blue and yellow stars represent
 1279 the location of samples collected on the CRT surfaces and intended for analysis in ³⁶Cl concentration and ²³⁰Th/U dating, respectively.
 1280 The relative sea level curve is from Waelbroeck et al. (2002).

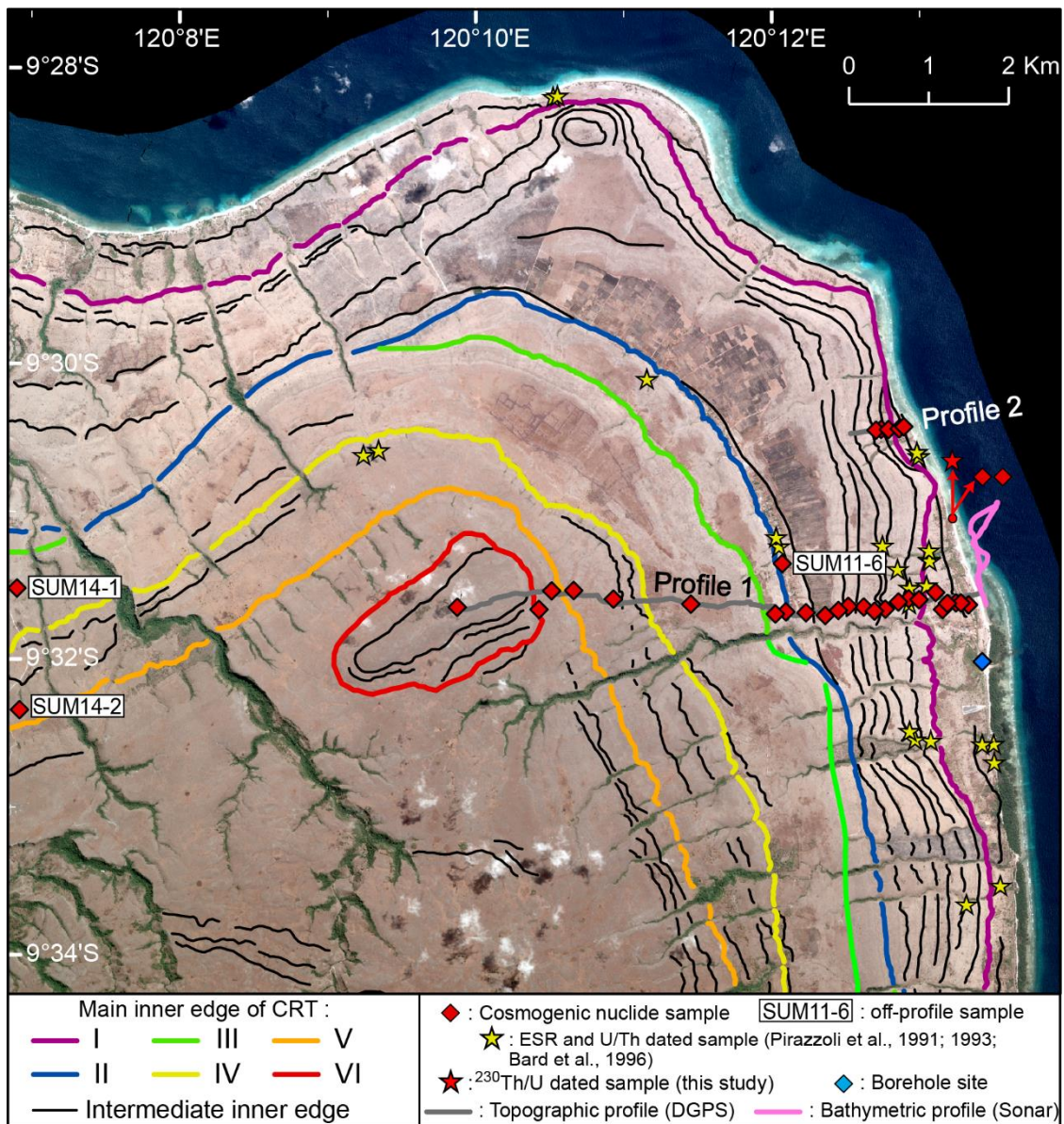


1281 **Fig. 3. A)** Geodynamics of SE Asia and location of Sumba Island (Indonesia). Plate
 1282 velocities indicated in relation to the Eurasia plate, from Nugroho et al. (2009),
 1283 elevation data from the Shuttle Radar Topography Mission (SRTM), and bathymetry

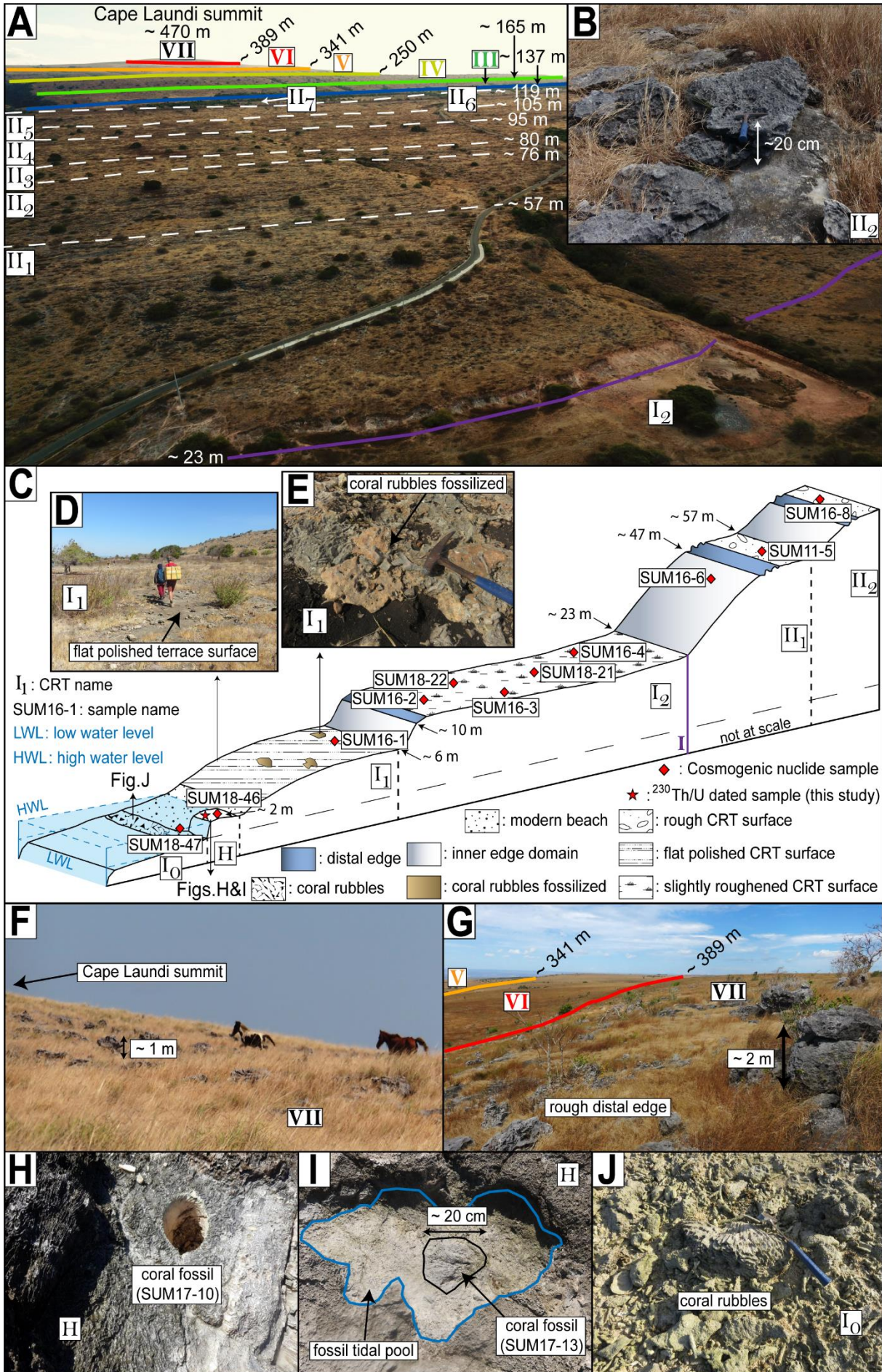
1284 data from the General Bathymetric Chart of Oceans (GEBCO), both at 90 m resolution.

1285 **B)** Digital elevation model (TanDEM-X, 13 m resolution) of Sumba Island.

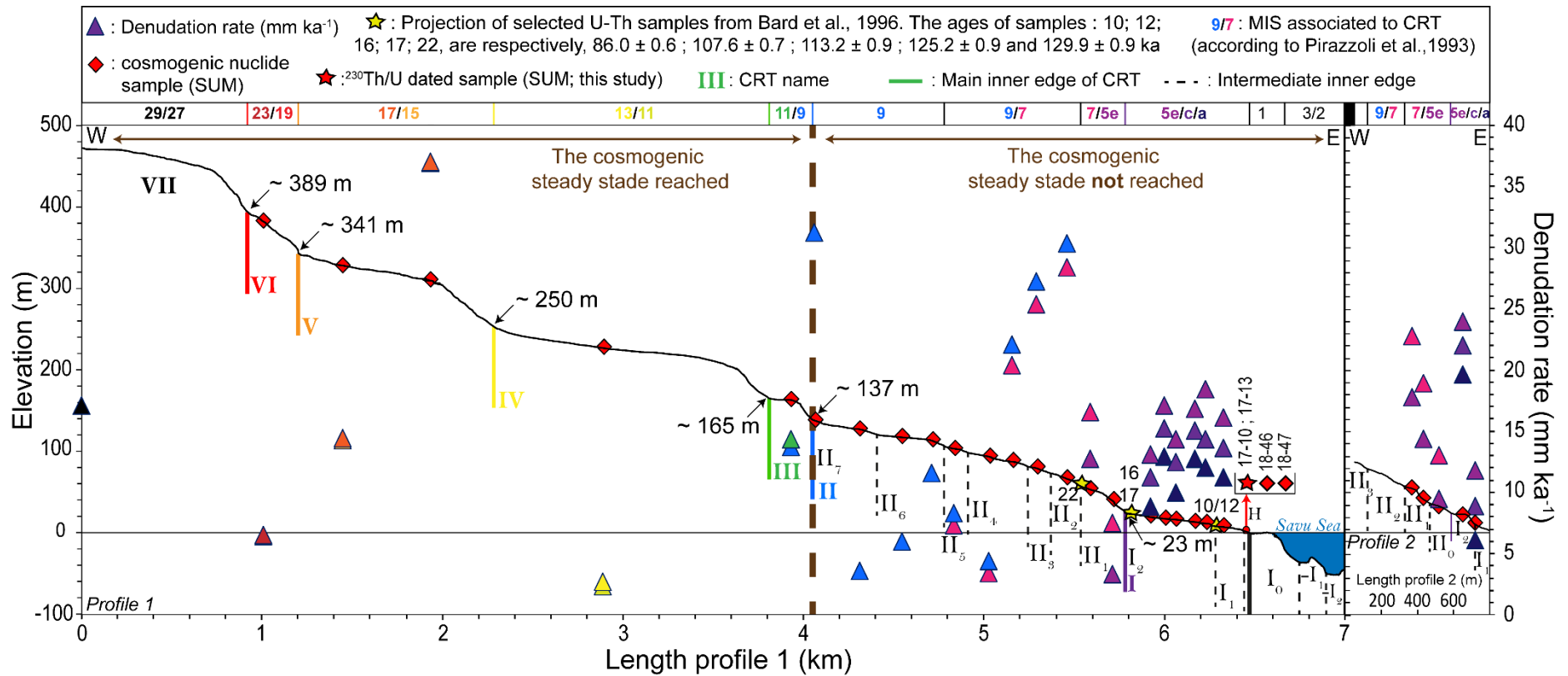
1286



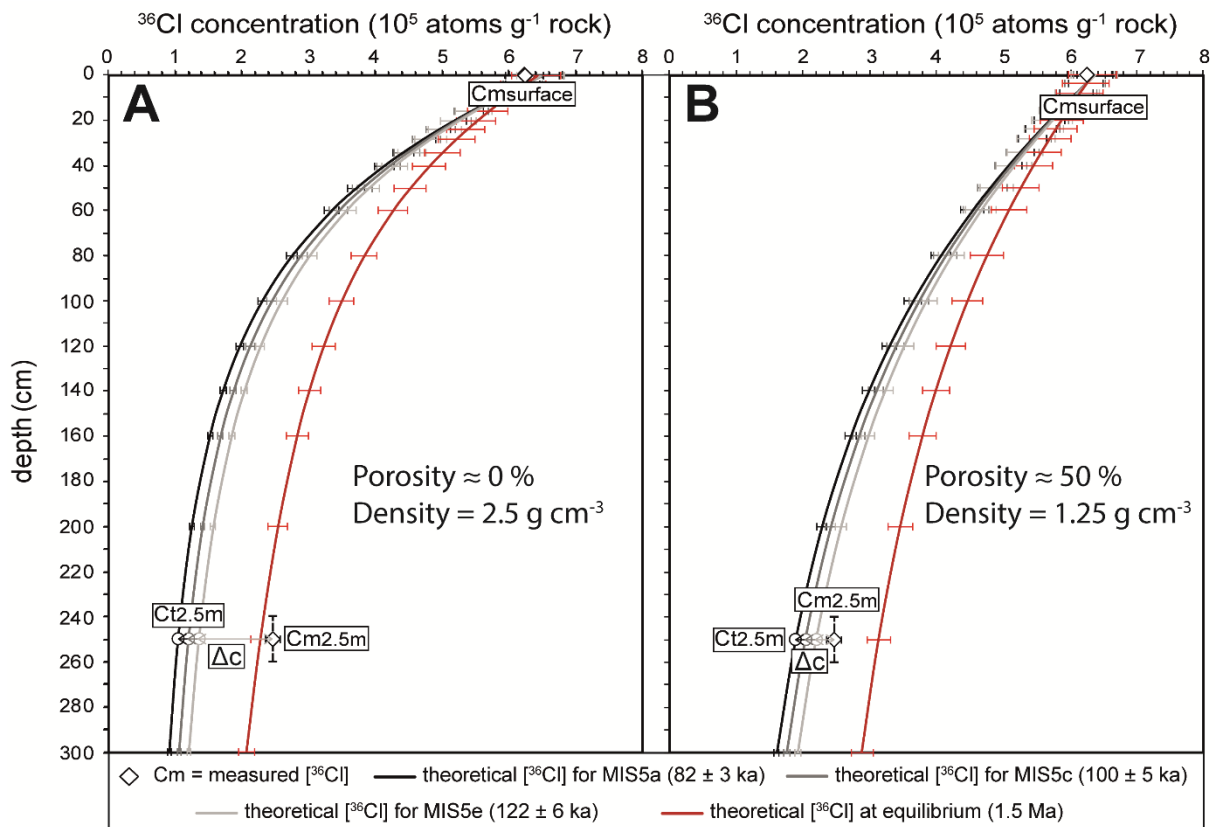
1287 **Fig. 4.** CRTs inner edges of the Cape Laundi sequence (Pleiades satellite imagery, 1
 1288 m resolution), and the location of samples, topographic and bathymetric profiles.



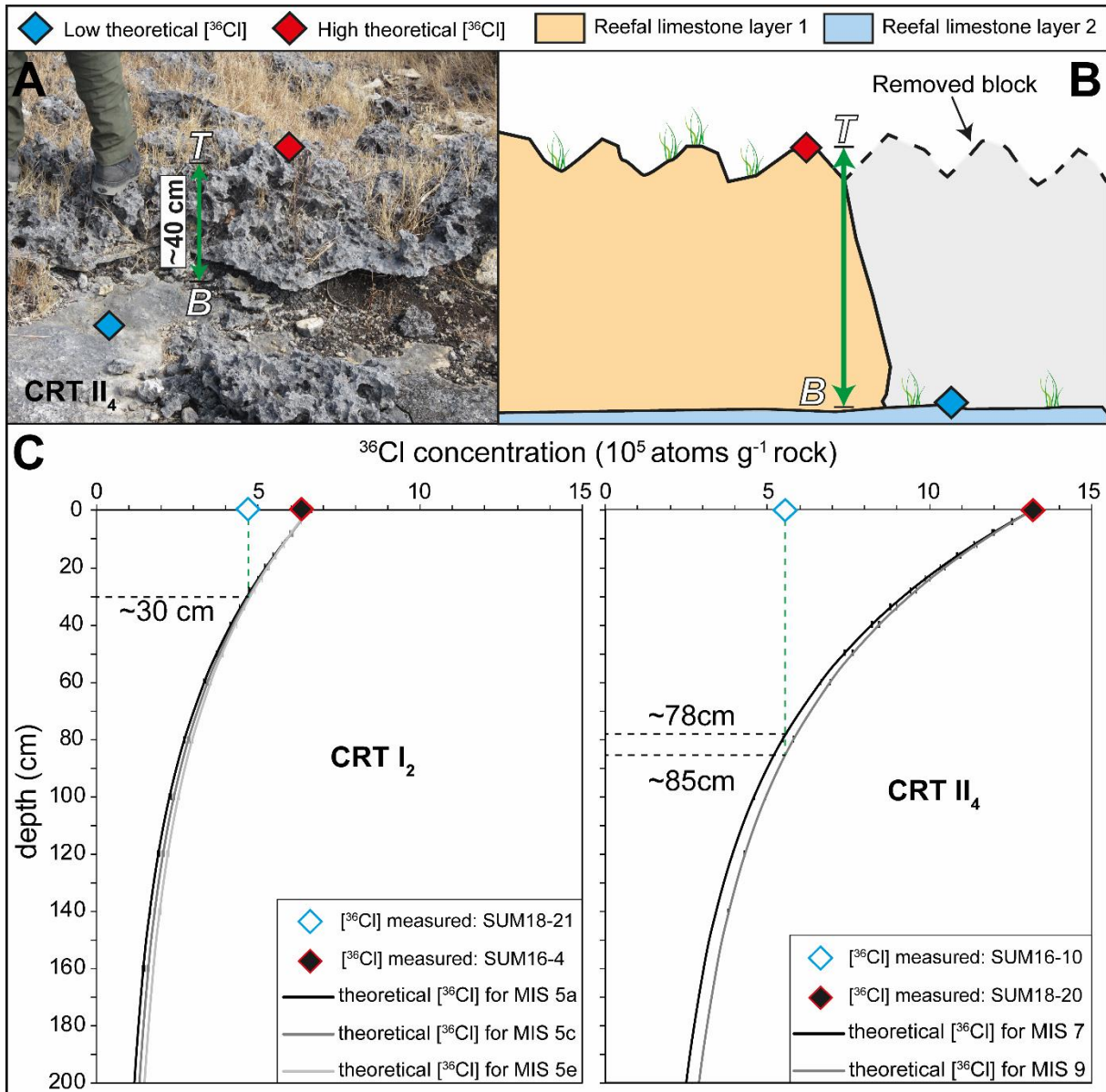
1290 **Fig. 5.** Pictures and interpretations of the Cap Laundi CRTs sequence. The elevations
1291 result from the DGPS profile. **A)** Aerial photo of Cape Laundi showing the staircase
1292 coastal landscape. **B)** CRT II₂ surface. **C)** Schematic 3D diagram of the lowest CRTs,
1293 with locations of Figs. 5D; 5E; 5H; 5I; 5J. **D)** Smooth flat surface of CRT I₁. **E)** Fossil
1294 coral rubbles cemented within the reefal limestones outcropping on the CRT I₁ surface.
1295 **F)** Cape Laundi summit. **G)** Distal edge of CRT VII. **H)** Sample SUM17-10. **I)** Sample
1296 SUM17-13). **J)** Coral rubbles on the modern reef flat (CRT I₀).



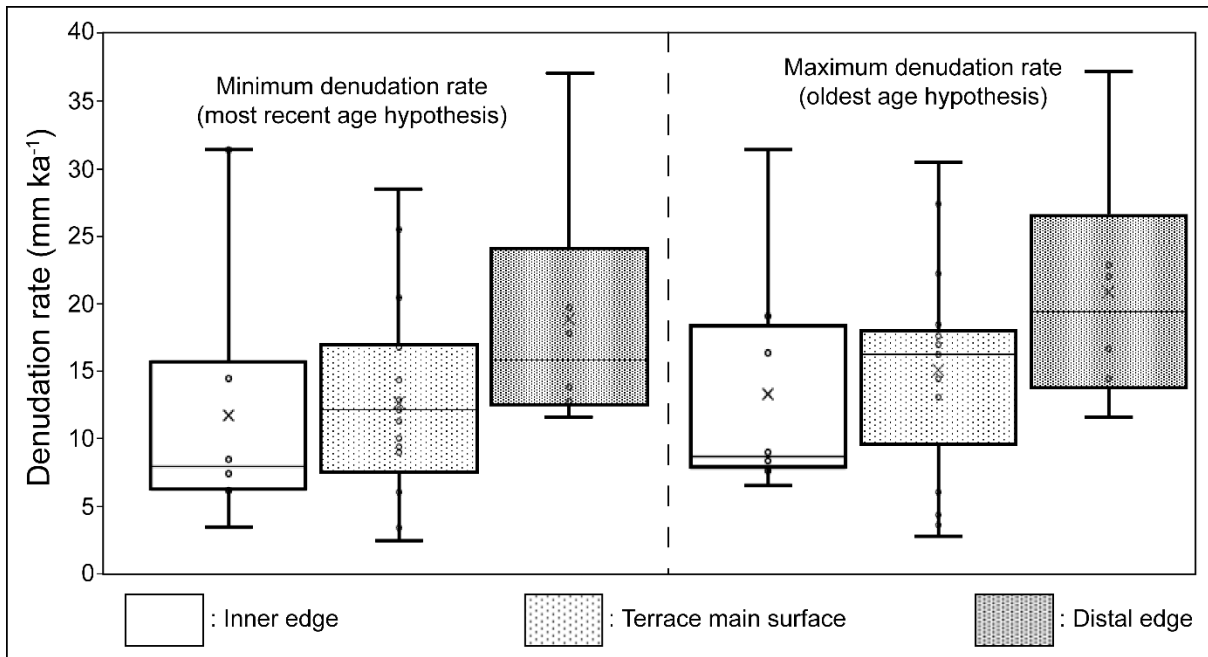
1297 **Fig. 6.** Altimetric profiles (DGPS and sonar) at Cape Laundi, showing the calculated denudation rates with various age hypotheses
 1298 (the colors of the triangles correspond to different age hypotheses), as well as location and ages of U/Th samples (Bard et al., 1996;
 1299 this study).



1300 **Fig. 7.** Surface (C_{msurface}) and $2.5 \pm 0.1 \text{ m}$ ($C_{\text{m2.5m}}$) depth ^{36}Cl concentration of the
 1301 borehole within CRT I_1 for a porosity of **A)** 50 % (i.e., density = 1.25 g cm^{-3}) and **B)** 0%
 1302 (density = 2.5 g cm^{-3}). Theoretical ^{36}Cl concentration curves as a function of depth and
 1303 MIS and age hypotheses. ΔC is the difference between measured ^{36}Cl ($C_{\text{m2.5m}}$) and
 1304 theoretical concentrations at $2.5 \pm 0.1 \text{ m}$ depth ($C_{\text{t2.5m}}$).



1305 **Fig. 8.** ^{36}Cl concentration variations at the scale of a CRT. **A)** Epikarstification on the
 1306 surface of CRT II₄. **B)** Schematic cross-sectional view of Figure 7A. *T* and *B*
 1307 correspond to the top and bottom of the reefal limestone layer 1, respectively. **C)**
 1308 Theoretical ^{36}Cl concentration curves of depth for 2 samples pairs (SUM18-21/16-4
 1309 and SUM18-20/16-10) as a function of depth and MIS and age hypotheses, assuming
 1310 that the ages of reefal bioconstruction and exposure duration are synchronous, as
 1311 proposed by Pirazzoli et al. (1991; 1993).



1312 **Fig. 9.** Boxplots of denudation rates, calculated with the most recent and oldest age
 1313 hypothesis, classified by morphological zone. The crosses, inner bars, circles, upper,
 1314 and lower outer bars represent the average, median, data, maximum and minimum
 1315 value for ^{36}Cl concentrations, respectively.

1316

1317 **Tables**

Sample (SUM)	Sample information						Sample composition		²³⁰ Th/U chemistry							
	Coral species	CRT	Morphology location	Longitude (E)	Latitude (N)	Elevation (m)	Calcite (%)	Aragonite (%)	²³⁸ U (μg/g)	²³² Th (ng/g)	(²³⁴ U/ ²³⁸ U)	(²³⁰ Th/ ²³⁸ U)	age uncorrected (ka)	age corrected (ka)	MIS	(²³⁴ U/ ²³⁸ U)initial
17-10	<i>Pseudodiploria clivosa</i>	H	Distal edge	120.221	-9.52	2.0 ± 0.5	< 1	> 99	2.37 ± 0.01	1.080 ± 0.006	1.14627 ± 0.00041	0.05584 ± 0.00020	5.460 ± 0.020	5.448 ± 0.02	1	1.14854 ± 0.00040
17-13	<i>Mussismilia leptophylla</i>	H	Distal edge	120.221	-9.52	2.0 ± 0.5	< 1	> 99	3.02 ± 0.02	1.281 ± 0.007	1.1404 ± 0.0003	0.02199 ± 0.00010	2.1359 ± 0.0083	2.1252 ± 0.0098	1	1.14126 ± 0.00030

1318 **Table 1.** Results of ²³⁰Th/U dating of samples SUM17-10 and SUM17-13.

1319

1320

1321

1322

1323

1324

1325

1326

1327

1328

1329

1330

1331

Sample (SUM)	Sample location, elevation, slope and Mean Annual Precipitation (MAP)							Sample composition			AMS result
	DGPS profile	CRT name	Longitude (E)	Latitude (N)	Elevation (m)	Slope (°)	MAP (mm yr ⁻¹)	Cl (target fraction) (ppm ± 0.12)	CaO (target fraction) (wt% ± 0.25)	MgO (bulk rock) (wt%)	[³⁶ Cl] (10 ⁵ atom g ⁻¹ rock)
16-1	Profile 1	I1	120.2222	-9.5272	8.4 ± 0.5	0.0	722.8	26.23	55.24	0.39	5.95 ± 0.14
16-2	Profile 1	I2	120.2213	-9.5270	12.5 ± 0.5	2.6	722.3	15.08	54.82	0.47	5.43 ± 0.13
18-22	Profile 1	I2	120.2208	-9.5270	14.4 ± 0.5	1.5	723.3	14.17	52.06	0.57	4.82 ± 0.11
16-3	Profile 1	I2	120.2198	-9.5271	17.4 ± 0.5	3.8	727.3	12.26	56.61	0.36	6.1 ± 0.14
18-21	Profile 1	I2	120.2193	-9.5278	18.5 ± 0.5	1.5	739.9	6.29	54.34	0.32	4.69 ± 0.10
16-4	Profile 1	I2	120.2185	-9.5258	20.4 ± 0.5	1.7	723.9	14.94	55.77	0.29	6.26 ± 0.14
16-6	Profile 1	II1	120.2166	-9.5266	40.7 ± 0.5	14.9	750.7	3.07	55.80	0.34	9.7 ± 0.22
11-5	Profile 1	II1	120.2154	-9.5266	54.4 ± 0.5	4.2	760.1	18.97	53.62	0.68	6.33 ± 0.14
16-8	Profile 1	II2	120.2143	-9.5269	67.5 ± 0.5	4.5	774.6	6.49	55.51	0.47	4.45 ± 0.10
16-9	Profile 1	II3	120.2128	-9.5277	80.2 ± 0.5	4.0	797.7	8.81	55.37	0.31	4.8 ± 0.11
16-10	Profile 1	II4	120.2116	-9.5279	88.1 ± 0.5	3.1	811.6	2.89	55.14	0.15	5.53 ± 0.12
18-20	Profile 1	II4	120.2104	-9.5275	94.4 ± 0.5	3.6	816.7	1.75	52.58	0.40	13.17 ± 0.31
18-19	Profile 1	II5	120.2086	-9.5274	104.0 ± 0.5	3.3	831.3	3.67	53.59	0.28	9.54 ± 0.19
18-18	Profile 1	II6	120.2075	-9.5279	113.9 ± 0.5	3.6	847.2	2.47	52.72	0.36	7.63 ± 0.17
18-17	Profile 1	II6	120.2060	-9.5284	117.9 ± 0.5	1.5	867.0	4.32	52.75	0.34	11.47 ± 0.23
18-16	Profile 1	II7	120.2039	-9.5281	127.8 ± 0.5	3.6	881.6	5.57	47.47	0.42	13.57 ± 0.26
18-15	Profile 1	II7	120.2016	-9.5280	138.6 ± 0.5	8.2	901.0	3.16	50.46	0.30	3.80 ± 0.08
18-14	Profile 1	III	120.2004	-9.5283	163.0 ± 0.5	6.0	913.9	2.16	54.33	0.24	7.20 ± 0.16
18-37	Profile 1	IV	120.1909	-9.5272	227.1 ± 0.5	6.2	987.1	4.42	51.70		20.00 ± 0.37
18-36	Profile 1	V	120.1822	-9.5266	309.5 ± 1.5	7.3	1059.6	2.87	52.19	0.20	4.04 ± 0.09
18-35	Profile 1	V	120.1777	-9.5256	327.2 ± 1.5	8.8	1073.7	2.23	53.19	0.25	8.50 ± 0.17
18-31	Profile 1	VI	120.1738	-9.5278	380.5 ± 1.5	3.5	1101.7	2.43	53.20	0.46	15.00 ± 0.28
18-33	Profile 1	VII	120.1646	-9.5275	471.6 ± 1.5	2.7	1109.8	4.06	51.42	0.20	8.01 ± 0.17
18-24	Profile 2	I1	120.2149	-9.5072	14.7 ± 0.5	14.4	765.6	38.37	52.12	0.51	7.26 ± 0.16
18-25	Profile 2	I2	120.2144	-9.5074	25.8 ± 0.5	3.1	767.4	7.37	52.29	0.29	3.68 ± 0.08
18-26	Profile 2	II0	120.2132	-9.5075	35.2 ± 0.5	7.0	774.4	49.08	51.88	0.63	8.31 ± 0.21
18-28	Profile 2	II1	120.2123	-9.5075	43.3 ± 0.5	10.6	779.6	3.96	53.32	0.50	5.11 ± 0.11
18-27	Profile 2	II1	120.2118	-9.5076	56.1 ± 0.5	12.1	782.4	9.24	51.62	0.29	5.11 ± 0.11
Cmsurface	Borehole	I1	120.2237	-9.5336	2.8 ± 0.5	0.0	790.6	12.26	56.61	0.36	6.23 ± 0.14
Cm2.5m	Borehole	I1	120.2237	-9.5336	-2.5 ± 0.1			18.15	52.49	0.75	2.46 ± 0.06
18-46	Off profile	I1	120.2207	-9.5179	2.0 ± 0.5	0.0	638.9	245.15	47.14	2.67	0.38 ± 0.04
18-47	Off profile	I0	120.2207	-9.5179	0.0	0.0	638.9	178.84	49.93	1.43	0.30 ± 0.03
11-6	Off profile	II6	120.2009	-9.5217	149.3 ± 0.5	2.1	830.8	3.38	55.33	0.38	10.82 ± 0.23
14-2	Off profile	IV	120.1139	-9.5274	210.8 ± 0.5	3.5	1094.4	2.22	55.33	0.26	7.07 ± 0.15
14-2	Off profile	V	120.1141	-9.5407	293.9 ± 1.5	3.4	1142.8	1.97	55.69	0.14	8.27 ± 0.18

1332 **Table 2.** Bedrock sample information, location, elevation, chemical composition, and AMS ³⁶Cl results. Mean annual precipitation
1333 (MAP) values are TRMM data (e.g., Kummerow et al., 2000).

Sample (SUM)	Morphology location	AMS result [²⁶ C]	Hypothesis 1			Hypothesis 2			Hypothesis 3			Mean denudation rate (mm ka ⁻¹)	Integration time (ka)
			MIS	Exposure duration (ka)	Denudation rate (mm ka ⁻¹)	MIS	Exposure duration (ka)	Denudation rate (mm ka ⁻¹)	MIS	Exposure duration (ka)	Denudation rate (mm ka ⁻¹)		
16-1	Terrace main surface	5.95 ± 0.14	5a	82 ± 3	11.3 ± 0.1	5c	100 ± 5	13.7 ± 0.1	5e	122 ± 6	16.2 ± 0.1	13.7 ± 2.5	44.7 ± 8.0
16-2	Terrace main surface	5.43 ± 0.13	5a	82 ± 3	12.1 ± 0.1	5c	100 ± 5	14.4 ± 0.1	5e	122 ± 6	18.4 ± 0.1	15.0 ± 3.2	41.2 ± 8.5
18-22	Terrace main surface	4.82 ± 0.11	5a	82 ± 3	12.8 ± 0.4	5c	100 ± 5	175.1 ± 0.4	5e	122 ± 6	16.9 ± 0.4	14.9 ± 2.1	40.7 ± 5.7
16-3	Terrace main surface	6.1 ± 0.14	5a	82 ± 3	10.0 ± 0.1	5c	100 ± 5	12.5 ± 0.1	5e	122 ± 6	14.4 ± 0.1	12.3 ± 2.2	49.9 ± 9.3
18-21	Terrace main surface	4.69 ± 0.10	5a	82 ± 3	13.0 ± 0.4	5c	100 ± 5	15.2 ± 0.4	5e	122 ± 6	17.1 ± 0.4	15.1 ± 2.1	40.3 ± 5.7
16-4	Terrace main surface	6.26 ± 0.14	5a	82 ± 3	8.9 ± 0.1	5c	100 ± 5	11.3 ± 0.1	5e	122 ± 6	13.1 ± 0.1	11.1 ± 2.1	55.5 ± 11.3
16-6	Inner edge	9.7 ± 0.22	5e	122 ± 6	3.4 ± 0.0(2)	7e	239.5 ± 8.5	7.6 ± 0.0(2)				5.5 ± 2.9	127.9 ± 68.6
11-5	Distal edge	6.33 ± 0.14	5e	122 ± 6	12.8 ± 0.1	7e	239.5 ± 8.5	16.7 ± 0.1				14.7 ± 2.8	41.6 ± 7.8
16-8	Terrace main surface	4.45 ± 0.10	7e	239.5 ± 8.5	28.4 ± 0.2	9e	325 ± 18.5	30.4 ± 0.2				29.4 ± 1.4	20.4 ± 1.0
16-9	Terrace main surface	4.8 ± 0.11	7e	239.5 ± 8.5	25.4 ± 0.2	9e	325 ± 18.5	27.3 ± 0.2				26.4 ± 1.3	22.8 ± 1.1
16-10	Terrace main surface	5.53 ± 0.12	7e	239.5 ± 8.5	20.4 ± 0.1	9e	325 ± 18.5	22.1 ± 0.1				21.3 ± 1.2	28.3 ± 1.6
18-20	Terrace main surface	13.17 ± 0.31	7e	239.5 ± 8.5	3.4 ± 0.1	9e	325 ± 18.5	4.4 ± 0.1				3.9 ± 0.7	156.0 ± 26.8
18-19	Inner edge	9.54 ± 0.19	7e	239.5 ± 8.5	7.4 ± 0.2	9e	325 ± 18.5	8.3 ± 0.2				7.8 ± 0.7	76.8 ± 6.4
18-18	Distal edge	7.63 ± 0.17	9e	325 ± 18.5	11.6 ± 0.3							11.6 ± 0.3	51.7 ± 0.1
18-17	Terrace main surface	11.47 ± 0.23	9e	325 ± 18.5	6.0 ± 0.1							6.0 ± 0.1	99.5 ± 0.1
18-16	Terrace main surface	13.57 ± 0.26	9e	325 ± 18.5	3.6 ± 0.1							3.6 ± 0.1	164.8 ± 0.1
18-15	Inner edge	3.80 ± 0.08	9e	325 ± 18.5	31.3 ± 0.8							31.3 ± 0.8	19.2 ± 0.1
18-14	Distal edge	7.20 ± 0.16	9e	325 ± 18.5	13.8 ± 0.4	11c	390 ± 30	14.4 ± 0.4				14.1 ± 0.4	42.5 ± 1.4
18-37	Terrace main surface	20.00 ± 0.37	11c	390 ± 30	2.3 ± 0.1	13a	495 ± 15	2.8 ± 0.1				2.5 ± 0.3	237.3 ± 27.0
18-36	Distal edge	4.04 ± 0.09	15e	610 ± 10	37.0 ± 0.9	17c	695 ± 15	37.1 ± 0.9				37.1 ± 0.1	16.2 ± 0.3
18-35	Terrace main surface	8.50 ± 0.17	15e	610 ± 10	14.3 ± 0.3	17c	685 ± 15	14.4 ± 0.3				14.4 ± 0.1	41.8 ± 0.3
18-31	Inner edge	15.00 ± 0.28	19	780 ± 10	6.4 ± 0.1	21	850 ± 15	6.5 ± 0.1	23	910 ± 10	6.6 ± 0.1	6.5 ± 0.1	92.4 ± 0.8
18-33	Terrace main surface	8.01 ± 0.17	27	980 ± 5	17.1 ± 0.4	29	1020 ± 10	17.2 ± 0.4				17.2 ± 0.0(1)	35.0 ± 0.1
18-24	Inner edge	7.26 ± 0.16	5a	82 ± 3	6.1 ± 0.2	5c	100 ± 5	8.9 ± 0.2	5e	122 ± 6	10.8 ± 0.2	8.6 ± 2.4	73.8 ± 22.1
18-25	Distal edge	3.68 ± 0.08	5a	82 ± 3	19.7 ± 0.5	5c	100 ± 5	22.0 ± 0.5	5e	122 ± 6	24.0 ± 0.2	21.9 ± 2.2	27.6 ± 2.8
18-26	Terrace main surface	8.31 ± 0.21	5e	122 ± 6	9.4 ± 0.2	7e	239.5 ± 8.5	13.0 ± 0.2				11.2 ± 2.6	55.1 ± 12.8
18-28	Inner edge	5.11 ± 0.11	5e	122 ± 6	14.4 ± 0.4	7e	239.5 ± 8.5	19.0 ± 0.4				16.7 ± 3.3	36.6 ± 7.1
18-27	Distal edge	5.11 ± 0.11	5e	122 ± 6	17.8 ± 0.5	7e	239.5 ± 8.5	22.8 ± 0.5				20.3 ± 3.5	30.0 ± 5.3
18-46	Distal edge	0.38 ± 0.04	Holocene	2.13 ± 0.01	279.0 ± 0.4	Holocene	5.45 ± 0.02	581.0 ± 0.4				430 ± 214	1.6 ± 2.8
11-6	Inner edge	10.82 ± 0.23	9e	325 ± 18.5	8.4 ± 0.2							8.4 ± 0.2	71.4 ± 0.1
14-1	Terrace main surface	7.07 ± 0.15	11c	390 ± 30	16.8 ± 0.4	13a	495 ± 15	17.5 ± 0.4				17.1 ± 0.5	35.0 ± 1.1
14-2	Inner edge	8.27 ± 0.18	15e	610 ± 10	16.1 ± 0.4	17c	685 ± 15	16.3 ± 0.4				16.2 ± 0.1	37.0 ± 0.3

1334

1335 **Table 3.** Morphology location and calculated denudation rates from the ^{36}Cl concentrations and the different MIS and age hypotheses,
1336 assuming that the ages of reefal bioconstruction and exposure duration are synchronous, for each CRT of the sequence as proposed
1337 by Pirazzoli et al. (1991; 1993). The MIS ages and their uncertainties are derived from Cutler et al. (2003) and Murray-Wallace and
1338 Woodroffe (2014). Denudation rate uncertainties are calculated by standard error propagation, including uncertainties from production
1339 rates, ages, and AMS measurements. Mean denudation rate uncertainties are calculated using the standard deviation.

Porosity %	Density (g cm ⁻³)	Ed		Denudation rate (mm ka ⁻¹)	Ct2.5m (10 ⁵ atoms g rock ⁻¹)	Δc (10 ⁵ atoms g rock ⁻¹)	Ed Δc ka
		MIS	ka				
50	1.25	5a	82 ± 3	20.0 ± 0.2	1.88 ± 0.03	0.58 ± 0.15	5.4 ± 1.3
		5c	100 ± 5	24.9 ± 0.2	2.02 ± 0.03	0.44 ± 0.15	4.0 ± 1.2
		5e	122 ± 6	28.6 ± 0.3	2.18 ± 0.03	0.28 ± 0.15	2.6 ± 1.2
0	2.5	5a	82 ± 3	9.5 ± 0.2	1.05 ± 0.03	1.41 ± 0.15	13.8 ± 1.3
		5c	100 ± 5	11.9 ± 0.2	1.19 ± 0.03	1.27 ± 0.15	12.5 ± 1.2
		5e	122 ± 6	13.8 ± 0.3	1.34 ± 0.03	1.15 ± 0.15	11.0 ± 1.2

1340 **Table 4.** Borehole ³⁶Cl theoretical concentrations and theoretical exposure duration within CRT I₁. Ed, MIS, Ct2.5m, Δc , Ed Δc ,
1341 correspond to the exposure duration for surface sample (Cmsurface), Marine Isotope Stage, ³⁶Cl theoretical concentration at 2.5 ±
1342 0.1 m depth (Ct2.5m) calculated from the ³⁶Cl measured concentration of the surface sample, the difference between ³⁶Cl measured
1343 (Cm2.5m) and theoretical concentrations at 2.5 ± 0.1 m depth (Ct2.5m), the theoretical exposure duration calculated from Δc ,
1344 respectively. The ages and their uncertainties are derived from Cutler et al. (2003) and Murray-Wallace and Woodroffe (2014).